J. Appl. Comput. Mech., xx(x) (2026) 1-18
DOI: 10.22055/jacm.2026.49382.5936

ISSN: 2383-4536
jacm.scu.ac.ir

Shahid Chamran University of Ahvaz

Journal of Applied and Computational Mechanics



Research Paper

A Symplectic-Analysis-Based Extended Finite Element Method for Bending of Bi-Material Plates with Interface Cracks

Wang Xu[1,2], Jinyan Chen[1,2], Youhan Xu[1], Linna Li[1,2], Dongwang Zhong[2]

[1] School of Physics and Mechanics, Wuhan University of Science and Technology, Wuhan, 430065, P. R. China
[2] Hubei Province Intelligent Blasting Engineering Technology Research Center, Wuhan, 430065, P. R. China

Received May 19 2026; Revised October 21 2026; Accepted for publication October 22 2026.
✉ Corresponding author: W. Xu (xuwang@wust.edu.cn)
© 2026 Published by Shahid Chamran University of Ahvaz

Abstract. Plate structures with interface cracks suffer from complex bending-fracture behavior due to material discontinuity, making accurate stress intensity factor (SIF) calculation critical for structural safety. This study proposes a symplectic-analysis-based extended finite element method (XFEM) for bending analysis of bi-material plates with interface cracks under Kirchhoff plate theory. Based on the Hamiltonian system, the symplectic analytical solution of plate bending is obtained, and orthogonal symplectic series terms related to stress singularity are constructed into enrichment functions for XFEM. The three-node triangular Discrete Kirchhoff Theory (DKT) element is adopted for discretization, with Heaviside and interface-improvement functions introduced to handle displacement and material property discontinuities, respectively. Furthermore, an interaction integral method tailored for evaluating SIFs in bi-material plate bending problems is developed, wherein the auxiliary fields are rigorously obtained from the symplectic analytical solution. Numerical simulations of square/rectangular plates with central/edge interface cracks under bending moment and uniform transverse load verify the model's accuracy and convergence. The method reveals that elastic modulus ratio, crack length/inclination, and Poisson's ratio significantly affect SIFs, providing reliable data for bi-material plate fracture assessment.

Keywords: Bending plate; Interface crack; Extended finite element method; Symplectic method; Interaction integral.

1. Introduction

Plate structures are extensively utilized across a range of engineering fields, including mechanical equipment, aerospace, vehicle engineering, and shipbuilding. In service, these structures are often subjected to lateral loads, resulting in bending deformation. The introduction of cracks or interfacial cracks can substantially compromise their load-bearing capacity. Consequently, the accurate determination of stress intensity factors (SIFs) at crack tips under bending conditions is crucial for the safety assessment and integrity evaluation of plate structures.

The stress intensity factor was first introduced by Irwin as a parameter to quantify the singularity of the stress field at a crack tip [1]. Subsequently, Williams [2] identified a stress singularity of order $r^{-1/2}$ at the tip of a bending crack in a homogeneous plate and provided the stress expressions for the near-tip field, laying an important theoretical foundation for later developments. Sih et al. [3] employed the complex-variable method to define the stress intensity factors (SIFs) for cracked Kirchhoff plates, thereby establishing a key parameter system for bending fracture in homogeneous plates. Wang [4] together with Hartranft and Sih [5] adopted Reissner plate theory and respectively applied integral equations and a novel Fredholm equation to demonstrate the significant effect of plate thickness on SIFs. Barsoum [6] derived a general-purpose bending element from a degenerate 20-node solid isoparametric element for linear fracture analysis of through-thickness cracks. Chen et al. [7] developed a finite-element alternating method based on classical plate theory, whereas Leung and Su [8] proposed a fractal two-level finite element method based on discrete Kirchhoff theory elements; both approaches enable high-precision solutions for bending-fracture problems in cracked homogeneous plates without requiring singular elements. Park and Atluri [9] extended the finite-element alternating method to determine SIFs for multiple collinear cracks in homogeneous plates under bending. Moës et al. [10] proposed a finite-element method for crack growth without remeshing, which, via the partition-of-unity technique, enabled mesh-independent simulation of crack propagation in homogeneous materials, overcoming the limitations of traditional mesh regeneration. Munaswamy and Pullela [11] employed the p-version finite-element method, achieving high-accuracy computation of bending SIFs for through-thickness cracks by elevating the interpolation order rather than refining the mesh. Leung et al. [12] proposed a hybrid method that combines symplectic analytical expansion with finite-element discretization (FEDSM) for direct and efficient calculation of SIFs in crack problems. Nguyen et al. [13] enhanced the extended integrated radial basis function (XiRBF) meshfree

Published online: November 26 2026

method for dynamic crack analysis in bending plate structures.

In engineering structures, bi-material plates can fulfill the requirements of diverse working environments and multifunctional designs, making them even more widely applicable. However, the bending-fracture behavior of such plates is more complex due to material discontinuity [14, 15]. Research in this area has increasingly focused on characterizing interface effects. Sih and Rice [16] first systematically derived the stress field at the tip of an interfacial crack in a bi-material plate under bending, revealing an oscillatory stress singularity and formulating a two-parameter equation to describe the crack-tip stress distribution. Perlman and Sih [17] utilized complex-variable theory to provide the first analytical solution for the SIFs of a circular-arc interfacial crack in a bi-material plate under bending. Chen and Hwu [18] constructed interpolation functions based on the displacement and stress fields of Sih and Rice to capture singular oscillatory behavior and defined new SIFs accordingly. Kakuno et al. [19] proposed an approach in which stress values at the crack tip are first computed using the finite element method and then used to evaluate the SIFs of an interfacial crack in a bi-material plate under bending via a scaling method. Oda et al. [20] computed SIFs for an edge interfacial crack under various material combinations and relative crack lengths and proposed an empirical expression for estimating SIFs under arbitrary material combinations. However, it should be noted that both studies [19, 20] focused on in-plane bending configurations, where the applied loads were parallel to the plate surface. Yao and Wang [21] introduced a symplectic dual system and employed the symplectic eigenfunction expansion method to address the bending problem of a bi-material sectorial Kirchhoff plate. Jiang et al. [22] pioneered the application of the generalized finite difference method (GFDM) to fracture-mechanics analysis of bi-material plates containing interfacial cracks, circumventing direct calculation of the oscillatory displacement and stress fields near the crack tip.

For thin plate bending analysis, the commonly used finite elements fall primarily into two categories. The first category comprises the DKQ series of quadrilateral elements [23] which include both four-node and eight-node variants. These elements employ high-order interpolation functions and strictly satisfy the continuity requirements of thin-plate bending deformation. Nevertheless, they still adopt conventional interpolation functions to independently approximate the deflection and the two normal rotations, after which the deflection and in-plane displacement modes are established based on the relationship between deflection and normal rotations as prescribed by Kirchhoff theory. However, in the context of Kirchhoff plate theory, the three degrees of freedom (the transverse deflection and the two rotations) are interdependent. Consequently, in finite element formulations, the conventional interpolation functions become unsuitable for thin-plate bending problems, as these degrees of freedom mutually constrain one another. This interdependence also presents notable challenges when applying the extended finite element method (XFEM) to such problems. The other category comprises three-node triangular elements based on the Discrete Kirchhoff Theory (DKT) [24]. Their main advantage lies in effectively mitigating the shear-locking issue common in thin-plate bending analysis by enforcing discrete Kirchhoff constraints. Furthermore, owing to the geometric flexibility of triangular meshes, DKT elements are particularly suitable for plates with irregular boundaries or complex geometries, thereby simplifying the discretization process. Batoz et al. [25] systematically evaluated the performance of three-node triangular plate-bending elements developed using three approaches: Discrete Kirchhoff Theory (DKT), Hybrid Stress Models (HSM), and Selective Reduced Integration (SRI). Their findings indicate that both DKT and HSM elements demonstrate high accuracy, robustness, and computational efficiency in thin-plate analyses.

The extended finite element method (XFEM) [26] offers a more flexible framework for crack analysis. By incorporating the Heaviside function [27, 28] and enrichment functions [29] into the standard displacement approximation, XFEM can handle displacement discontinuities independently of the mesh, thereby avoiding the need for mesh alignment with crack geometries and significantly simplifying the meshing process. However, the accuracy of XFEM strongly depends on the suitability of the enrichment functions. Existing enrichment functions are derived from classical elasticity solutions for cracks in single-material plates, such as the Williams series [30], and are therefore applicable only to bending-fracture analysis of homogeneous plates. For bi-material plate bending, current enrichment functions do not adequately account for the mechanical coupling effects at the bi-material interface and fail to accurately capture the characteristic stress singularity order and displacement field distribution specific to interfacial crack tips.

Based on the above research status and identified limitations, this study focuses on the bending fracture problem of bi-material plates containing interfacial cracks. Taking Kirchhoff plate bending theory as the mechanical foundation and integrating symplectic analytical theory [31] with the XFEM, a high-accuracy computational model for SIFs is established. The specific approach is as follows. First, to address the singular characteristics of interfacial cracks in bi-material systems, a symplectic analytical solution for plate bending is derived within a Hamiltonian framework [32]. The symplectic series solution possesses orthogonality, thereby ensuring reliable convergence. By analyzing the source of the stress singularity, the symplectic series terms with eigenvalues less than 1 are extracted as enrichment functions (16 independent terms in total) to accurately capture the stress singularity at the crack tip. Second, the triangular DKT element is adopted as the fundamental discretization element, and its displacement approximation is modified as follows: for elements completely cut by the crack, the Heaviside function is introduced to handle the displacement discontinuity across the crack; for elements intersected by the material interface, an interface-improvement function defined based on nodal level-set values is incorporated to handle the abrupt change in mechanical properties; for crack-tip elements, symplectic analytical enrichment functions are introduced to describe the stress oscillation at the crack tip. It should be noted that the introduced symplectic analytical enrichment functions must simultaneously include those associated with the deflection and those associated with the rotations. On this basis, coordinate transformation is employed to address the calculation of the derivatives of the shape functions and enrichment functions. According to the principle of minimum potential energy, the element stiffness matrix and equivalent nodal load vector are derived, forming a directly implementable numerical scheme. Finally, the symplectic analytical solution is employed as the auxiliary field and combined with the real field obtained by XFEM. The interaction integral is evaluated through a domain integral around the crack tip, from which the mode I and mode II SIFs under bending loads are determined, thereby enabling an accurate analysis of the bending fracture behavior of bi-material plates with interfacial cracks.

2. Symplectic Analytical Enrichment Functions

Consider a bi-material plate containing an interface crack, which is subjected to out-of-plane bending loads, leading to bending deformation. The thickness of the plate is h, and the two materials are designated as M_1 and M_2, with elastic moduli $E^{(1)}$ and $E^{(2)}$, and Poisson's ratios $\upsilon^{(1)}$ and $\upsilon^{(2)}$, respectively.

The bending deflection solution for a bi-material plate with an interfacial crack under the Hamiltonian system is:

$$w=\sum_{j=1}^{M}a_j w_j^{(i)}+a_{M+1}+a_{M+2}r\sin\theta+a_{M+3}r\cos\theta \tag{1}$$

where M represents the number of terms in the symplectic analytical result, and its value can be determined according to the convergence of the calculation results during the computation. a_j are the coefficients of the symplectic analytical series, and the superscript (i) indicates the material region. Here,

$$w_j^{(i)}=r^{\mu_j+1}\left\{\frac{1}{D^{(i)}\left(1+\mu_j\right)\left(1-\upsilon^{(i)}\right)}\left[A_j^{(i)}\cos\left(1+\mu_j\right)\theta-B_j^{(i)}\sin\left(1+\mu_j\right)\theta\right]-\frac{1}{D^{(i)}\left(3+\upsilon^{(i)}+\mu_j-\upsilon^{(i)}\mu_j\right)}\left[C_j^{(i)}\cos\left(1-\mu_j\right)\theta-G_j^{(i)}\sin\left(1-\mu_j\right)\theta\right]\right\} \tag{2}$$

where $D^{(i)}=E^{(i)}h^3/12[1-(\upsilon^{(i)})^2]$ is the flexural rigidity, $A^{(i)}, B^{(i)}, C^{(i)}, G^{(i)}$ are unknown coefficients, and the relationships between them are presented in Appendix A. μ are the eigenvalues of the symplectic analytical series,

$$\mu_{4j+1}=\left(j+\frac{1}{2}\right)-\mathrm{si},\ \mu_{4j+2}=\left(j+\frac{1}{2}\right)+\mathrm{si},\ (j=0,1,2,\cdots) \tag{3}$$

and,

$$\mu_{4j+3}=\mu_{4j+4}=j+1,\ (j=0,1,2,\cdots) \tag{4}$$

where i is the imaginary unit,

$$s=-\frac{1}{2\pi}\ln\left(\frac{1-k}{1+k}\right),\ k=\frac{1}{2}\left[\frac{\left(\frac{1-\upsilon^{(1)}}{1-\upsilon^{(2)}}\right)\left(\frac{3+\upsilon^{(1)}}{3+\upsilon^{(2)}}\right)\left(1+\upsilon^{(2)}\right)-\lambda\left(1+\upsilon^{(1)}\right)}{\lambda+\left(\frac{1-\upsilon^{(1)}}{1-\upsilon^{(2)}}\right)\left(\frac{3+\upsilon^{(1)}}{3+\upsilon^{(2)}}\right)}\right],\ \lambda=\frac{D^{(2)}}{D^{(1)}}.$$

In Kirchhoff theory, three degrees of freedom are considered, namely the deflection w, the rotation angle θ_x about the x-axis, and the rotation angle θ_y about the y-axis. Their relationships are:

$$\begin{aligned}\theta_x&=\frac{\partial w}{\partial y}=\frac{\partial w}{\partial r}\sin\theta+\frac{1}{r}\frac{\partial w}{\partial\theta}\cos\theta\\ \theta_y&=-\frac{\partial w}{\partial x}=\frac{1}{r}\frac{\partial w}{\partial\theta}\sin\theta-\frac{\partial w}{\partial r}\cos\theta\end{aligned} \tag{5}$$

According to the relationships between stress, strain, and deflection, that is:

$$\sigma=\mathbf{D}\varepsilon \tag{6}$$

$$\varepsilon=-z\left[\frac{\partial^2 w}{\partial x^2},\frac{\partial^2 w}{\partial y^2},2\frac{\partial^2 w}{\partial x\partial y}\right]^{\mathrm{T}} \tag{7}$$

where,

$$\sigma=\left\{\sigma_x,\sigma_y,\tau_{xy}\right\}^{\mathrm{T}},\ \varepsilon=\left\{\varepsilon_x,\varepsilon_y,\gamma_{xy}\right\}^{\mathrm{T}},\ \mathbf{D}=\frac{E}{1-\upsilon^2}\begin{bmatrix}1&\upsilon&0\\ \upsilon&1&0\\ 0&0&(1-\upsilon)/2\end{bmatrix}.$$

It is known that stress singularity is caused by the terms with eigenvalues less than 1 in the deflection expression, and the orders of stress singularity are $1-\mu_1$ and $1-\mu_2$. At the crack tip, where $r\to 0$, the terms with eigenvalues less than 1 are the main terms of the deflection.

In the extended finite element formulation, the terms with eigenvalues less than 1 are taken as enrichment functions:

$$w=r^{\frac{3}{2}\mp\mathrm{si}}\left\{\frac{1}{D\left(\frac{3}{2}\mp\mathrm{si}\right)(1-\upsilon)}\left[A\cos\left(\frac{3}{2}\mp\mathrm{si}\right)\theta-B\sin\left(\frac{3}{2}\mp\mathrm{si}\right)\theta\right]-\frac{1}{D\left(\frac{7}{2}\mp\mathrm{si}+\upsilon-\upsilon\left(\frac{1}{2}\mp\mathrm{si}\right)\right)}\left[C\cos\left(\frac{1}{2}\pm\mathrm{si}\right)\theta-G\sin\left(\frac{1}{2}\pm\mathrm{si}\right)\theta\right]\right\} \tag{8}$$

The above equation contains 16 independent terms, which are, respectively:

$$\begin{aligned}&F^1=r^{3/2}\cos(s\ln r)\cos(3\theta/2)e^{s\theta},\ F^2=r^{3/2}\cos(s\ln r)\cos(3\theta/2)e^{-s\theta},\ F^3=r^{3/2}\sin(s\ln r)\sin(3\theta/2)e^{s\theta},\ F^4=r^{3/2}\sin(s\ln r)\sin(3\theta/2)e^{-s\theta}\\ &F^5=r^{3/2}\cos(s\ln r)\sin(3\theta/2)e^{s\theta},\ F^6=r^{3/2}\cos(s\ln r)\sin(3\theta/2)e^{-s\theta},\ F^7=r^{3/2}\sin(s\ln r)\cos(3\theta/2)e^{s\theta},\ F^8=r^{3/2}\sin(s\ln r)\cos(3\theta/2)e^{-s\theta}\\ &F^9=r^{3/2}\cos(s\ln r)\cos(\theta/2)e^{s\theta},\ F^{10}=r^{3/2}\cos(s\ln r)\cos(\theta/2)e^{-s\theta},\ F^{11}=r^{3/2}\sin(s\ln r)\sin(\theta/2)e^{s\theta},\ F^{12}=r^{3/2}\sin(s\ln r)\sin(\theta/2)e^{-s\theta}\\ &F^{13}=r^{3/2}\cos(s\ln r)\sin(\theta/2)e^{s\theta},\ F^{14}=r^{3/2}\cos(s\ln r)\sin(\theta/2)e^{-s\theta},\ F^{15}=r^{3/2}\sin(s\ln r)\cos(\theta/2)e^{s\theta},\ F^{16}=r^{3/2}\sin(s\ln r)\cos(\theta/2)e^{-s\theta}\end{aligned} \tag{9}$$

The above 16 enrichment functions inherit the oscillatory characteristics of the interfacial crack solution. As can be seen from Eqs. (6)-(8), the strength of the stress singularity at the crack tip under plate bending is $r^{-1/2}$. The imaginary part of the eigenvalue introduces the oscillatory factors $\cos(s\ln r)$ and $\sin(s\ln r)$ into the logarithmic term; only together with the angular dependence of $e^{\mp s\theta}$ and the angular variations of $\cos(3\theta/2)$, $\sin(3\theta/2)$, $\cos(\theta/2)$, and $\sin(\theta/2)$ can the coupling field near the crack tip of a bi-material interfacial crack be fully characterized. The additional enrichment functions corresponding to the rotation angles θ_x and θ_y each also contain 16 independent terms, which can be obtained using Eq. (5) and are denoted as F_x^j and F_y^j, $j=1,2,3,\cdots,16$.

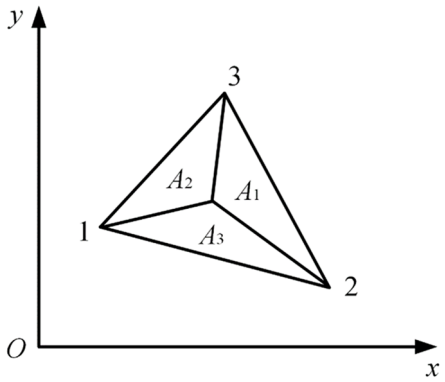


Fig. 1. Triangular Kirchhoff plate element.

3. Extended Finite Element Method

3.1. Three-node triangular Kirchhoff plate element

In this method, the triangular discrete Kirchhoff theory (DKT) element is used to discretize the thin plate. As shown in Fig. 1, the area coordinates of the three-node triangular plate elements can be expressed as:

$$L_i = \frac{1}{2A}(a_i + b_i x + c_i y), \qquad i = 1,2,3 \tag{10}$$

in which A is the area of the element, the coefficients are $a_1 = x_2y_3 - x_3y_2$, $a_2 = x_3y_1 - x_1y_3$, $a_3 = x_1y_2 - x_2y_1$, $b_1 = y_2 - y_3$, $b_2 = y_3 - y_1$, $b_3 = y_1 - y_2$, $c_1 = x_3 - x_2$, $c_2 = x_1 - x_3$, $c_3 = x_2 - x_1$.

The shape function is defined as:

$$\mathbf{N} = \begin{bmatrix} \mathbf{N}_1 & \mathbf{N}_2 & \mathbf{N}_3 \end{bmatrix} \tag{11}$$

where,

$$\mathbf{N}_k = \begin{bmatrix} N_k & N_{xk} & N_{yk} \end{bmatrix}, \ (k = 1,2,3)$$

$$N_1 = L_1 + L_1^2L_2 + L_1^2L_3 - L_1L_2^2 - L_1L_3^2, \ N_{x1} = b_2L_1^2L_3 - b_3L_1^2L_2 + \frac{1}{2}(b_2 - b_3)L_1L_2L_3, N_{y1} = c_2L_1^2L_3 - c_3L_1^2L_2 + \frac{1}{2}(c_2 - c_3)L_1L_2L_3,$$

$$N_2 = L_2 + L_2^2L_3 + L_2^2L_1 - L_2L_3^2 - L_2L_1^2, N_{x2} = b_3L_2^2L_1 - b_1L_2^2L_3 + \frac{1}{2}(b_3 - b_1)L_2L_3L_1, \ N_{y2} = c_3L_2^2L_1 - c_1L_2^2L_3 + \frac{1}{2}(c_3 - c_1)L_2L_3L_1$$

$$N_3 = L_3 + L_3^2L_1 + L_3^2L_2 - L_3L_1^2 - L_3L_2^2, N_{x3} = b_1L_3^2L_2 - b_2L_3^2L_1 + \frac{1}{2}(b_1 - b_2)L_3L_1L_2, N_{y3} = c_1L_3^2L_2 - c_2L_3^2L_1 + \frac{1}{2}(c_1 - c_2)L_3L_1L_2.$$

The displacement mode of the conventional finite element method is:

$$w = \sum_{i=1}^{3} N_i w_i + \sum_{i=1}^{3} N_{xi}\theta_{xi} + \sum_{i=1}^{3} N_{yi}\theta_{yi} \tag{12}$$

3.2. Extended finite element formulation

In the extended finite element method, the displacement formulation for the bending analysis of plates containing interfacial cracks can be constructed by introducing a Heaviside enrichment function in elements fully cut by the crack, crack-tip enrichment functions in elements containing the crack tip, and an interface enrichment function in elements intersected by the material interface:

$$\begin{aligned} w = &\sum_{i=1}^{3} N_i w_i + \sum_{i=1}^{3} N_{xi}\theta_{xi} + \sum_{i=1}^{3} N_{yi}\theta_{yi} + \sum_{i=1}^{3} N_i \left[\sum_{j=1}^{16} \left(F^j - F_i^j\right) a_i^j\right] + \sum_{i=1}^{3} N_{xi} \left[\sum_{j=1}^{16} \left(F_x^j - F_{xi}^j\right) b_i^j\right] + \sum_{i=1}^{3} N_{yi} \left[\sum_{j=1}^{16} \left(F_y^j - F_{yi}^j\right) c_i^j\right] \\ &+ \sum_{i=1}^{3} N_i \left[H(\mathbf{x}) - H(\mathbf{x}_i)\right] d_i + \sum_{i=1}^{3} N_i S(\mathbf{x}) e_i \end{aligned} \tag{13}$$

where a_i^j denotes the nodal unknowns associated with deflection enrichment, b_i^j and c_i^j represent the nodal unknowns corresponding to the enrichment of rotation about the x-axis and y-axis, respectively, d_i indicates the nodal unknowns related to Heaviside enrichment, and e_i refers to the nodal unknowns associated with interface discontinuity enrichment. The terms F_i^j, F_{xi}^j, F_{yi}^j represent the values of F^j, F_x^j, F_y^j at node i, respectively and,

$$H(\mathbf{x}) = \begin{cases} 1, & \left(\mathbf{x} - \mathbf{x}^*\right).\mathbf{n} > 0 \\ -1, & \left(\mathbf{x} - \mathbf{x}^*\right).\mathbf{n} < 0 \end{cases}$$

is the Heaviside function, **x** is the point under consideration, **x*** is its orthogonal projection onto the crack surface, and **n** is the unit outward normal to the crack surface at **x***. The function $S(\mathbf{x})=\sum_{i=1}^{3}N_i|\phi_i|-|\sum_{i=1}^{3}N_i\phi_i|$ is the enrichment function for elements intersected by material interface, and ϕ_i represents the level-set value of node i with respect to that interface.

To calculate the strain in the extended finite element formulation according to Eq. (7), the second-order partial derivatives of the deflection with respect to the Cartesian coordinates must be evaluated, given by:

$$\begin{aligned}\frac{\partial^2 w}{\partial x^2}=&\sum_{i=1}^{3}\frac{\partial^2 N_i}{\partial x^2}w_i+\sum_{i=1}^{3}\frac{\partial^2 N_{xi}}{\partial x^2}\theta_{xi}+\sum_{i=1}^{3}\frac{\partial^2 N_{yi}}{\partial x^2}\theta_{yi}\\&+\sum_{i=1}^{3}\sum_{j=1}^{16}\left[\frac{\partial^2 N_i}{\partial x^2}\left(F^j-F_i^j\right)+2\frac{\partial N_i}{\partial x}\frac{\partial F^j}{\partial x}+N_i\frac{\partial^2 F^j}{\partial x^2}\right]a_i^j\\&+\sum_{i=1}^{3}\sum_{j=1}^{16}\left[\frac{\partial^2 N_{xi}}{\partial x^2}\left(F_x^j-F_{xi}^j\right)+2\frac{\partial N_{xi}}{\partial x}\frac{\partial F_x^j}{\partial x}+N_{xi}\frac{\partial^2 F_x^j}{\partial x^2}\right]b_i^j\\&+\sum_{i=1}^{3}\sum_{j=1}^{16}\left[\frac{\partial^2 N_{yi}}{\partial x^2}\left(F_y^j-F_{yi}^j\right)+2\frac{\partial N_{yi}}{\partial x}\frac{\partial F_y^j}{\partial x}+N_{yi}\frac{\partial^2 F_y^j}{\partial x^2}\right]c_i^j\\&+\sum_{i=1}^{3}\frac{\partial^2 N_i}{\partial x^2}\left[H(\mathbf{x})-H(\mathbf{x}_i)\right]d_i+\sum_{i=1}^{3}\left[\frac{\partial^2 N_i}{\partial x^2}S(\mathbf{x})+2\frac{\partial N_i}{\partial x}\frac{\partial S(\mathbf{x})}{\partial x}+N_i\frac{\partial^2 S(\mathbf{x})}{\partial x^2}\right]e_i\end{aligned}\tag{14}$$

$$\begin{aligned}\frac{\partial^2 w}{\partial y^2}=&\sum_{i=1}^{3}\frac{\partial^2 N_i}{\partial y^2}w_i+\sum_{i=1}^{3}\frac{\partial^2 N_{xi}}{\partial y^2}\theta_{xi}+\sum_{i=1}^{3}\frac{\partial^2 N_{yi}}{\partial y^2}\theta_{yi}\\&+\sum_{i=1}^{3}\sum_{j=1}^{16}\left[\frac{\partial^2 N_i}{\partial y^2}\left(F^j-F_i^j\right)+2\frac{\partial N_i}{\partial y}\frac{\partial F^j}{\partial y}+N_i\frac{\partial^2 F^j}{\partial y^2}\right]a_i^j\\&+\sum_{i=1}^{3}\sum_{j=1}^{16}\left[\frac{\partial^2 N_{xi}}{\partial y^2}\left(F_x^j-F_{xi}^j\right)+2\frac{\partial N_{xi}}{\partial y}\frac{\partial F_x^j}{\partial y}+N_{xi}\frac{\partial^2 F_x^j}{\partial y^2}\right]b_i^j\\&+\sum_{i=1}^{3}\sum_{j=1}^{16}\left[\frac{\partial^2 N_{yi}}{\partial y^2}\left(F_y^j-F_{yi}^j\right)+2\frac{\partial N_{yi}}{\partial y}\frac{\partial F_y^j}{\partial y}+N_{yi}\frac{\partial^2 F_y^j}{\partial y^2}\right]c_i^j\\&+\sum_{i=1}^{3}\frac{\partial^2 N_i}{\partial y^2}\left[H(\mathbf{x})-H(\mathbf{x}_i)\right]d_i+\sum_{i=1}^{3}\left[\frac{\partial^2 N_i}{\partial y^2}S(\mathbf{x})+2\frac{\partial N_i}{\partial y}\frac{\partial S(\mathbf{x})}{\partial y}+N_i\frac{\partial^2 S(\mathbf{x})}{\partial y^2}\right]e_i\end{aligned}\tag{15}$$

$$\begin{aligned}\frac{\partial^2 w}{\partial x\partial y}=&\sum_{i=1}^{3}\frac{\partial^2 N_i}{\partial x\partial y}w_i+\sum_{i=1}^{3}\frac{\partial^2 N_{xi}}{\partial x\partial y}\theta_{xi}+\sum_{i=1}^{3}\frac{\partial^2 N_{yi}}{\partial x\partial y}\theta_{yi}\\&+\sum_{i=1}^{3}\sum_{j=1}^{16}\left[\frac{\partial^2 N_i}{\partial x\partial y}\left(F^j-F_i^j\right)+\frac{\partial N_i}{\partial x}\frac{\partial F^j}{\partial y}+\frac{\partial N_i}{\partial y}\frac{\partial F^j}{\partial x}+N_i\frac{\partial^2 F^j}{\partial x\partial y}\right]a_i^j\\&+\sum_{i=1}^{3}\sum_{j=1}^{16}\left[\frac{\partial^2 N_{xi}}{\partial x\partial y}\left(F_x^j-F_{xi}^j\right)+\frac{\partial N_{xi}}{\partial x}\frac{\partial F_x^j}{\partial y}+\frac{\partial N_{xi}}{\partial y}\frac{\partial F_x^j}{\partial x}+N_{xi}\frac{\partial^2 F_x^j}{\partial x\partial y}\right]b_i^j\\&+\sum_{i=1}^{3}\sum_{j=1}^{16}\left[\frac{\partial^2 N_{yi}}{\partial x\partial y}\left(F_y^j-F_{yi}^j\right)+\frac{\partial N_{yi}}{\partial x}\frac{\partial F_y^j}{\partial y}+\frac{\partial N_{yi}}{\partial y}\frac{\partial F_y^j}{\partial x}+N_{yi}\frac{\partial^2 F_y^j}{\partial x\partial y}\right]c_i^j\\&+\sum_{i=1}^{3}\frac{\partial^2 N_i}{\partial x\partial y}\left[H(\mathbf{x})-H(\mathbf{x}_i)\right]d_i+\sum_{i=1}^{3}\left[\frac{\partial^2 N_i}{\partial x\partial y}S(\mathbf{x})+\frac{\partial N_i}{\partial x}\frac{\partial S(\mathbf{x})}{\partial y}+\frac{\partial N_i}{\partial y}\frac{\partial S(\mathbf{x})}{\partial x}+N_i\frac{\partial^2 S(\mathbf{x})}{\partial x\partial y}\right]e_i\end{aligned}\tag{16}$$

In the formulations above, the derivatives of the shape functions with respect to Cartesian coordinates must be transformed into derivatives with respect to area coordinates, while the derivatives of the enrichment and interface-enrichment functions are converted from Cartesian to polar coordinates. The corresponding relationships are:

$$\begin{Bmatrix}\partial/\partial x\\ \partial/\partial y\end{Bmatrix}=\frac{1}{2\Delta}\begin{bmatrix}b_1 & b_2\\ c_1 & c_2\end{bmatrix}\begin{Bmatrix}\partial/\partial L_1\\ \partial/\partial L_2\end{Bmatrix}\tag{17}$$

$$\begin{Bmatrix}\partial^2/\partial x^2\\ \partial^2/\partial y^2\\ 2\partial^2/\partial x\partial y\end{Bmatrix}=\frac{1}{4\Delta^2}\mathbf{T}\begin{Bmatrix}\partial^2/\partial L_1^2\\ \partial^2/\partial L_2^2\\ \partial^2/\partial L_1\partial L_2\end{Bmatrix}\tag{18}$$

$$\begin{Bmatrix}\partial/\partial x\\ \partial/\partial y\end{Bmatrix}=\begin{bmatrix}\cos\theta & -\sin\theta/r\\ \sin\theta & \cos\theta/r\end{bmatrix}\begin{Bmatrix}\partial/\partial r\\ \partial/\partial\theta\end{Bmatrix}\tag{19}$$

$$\begin{aligned}\frac{\partial^2}{\partial x^2}&=\cos^2\theta\frac{\partial^2}{\partial r^2}-\frac{\sin 2\theta}{r}\frac{\partial^2}{\partial r\partial\theta}+\frac{\sin^2\theta}{r}\frac{\partial}{\partial r}+\frac{\sin 2\theta}{r^2}\frac{\partial}{\partial\theta}+\frac{\sin^2\theta}{r^2}\frac{\partial^2}{\partial\theta^2}\\\frac{\partial^2}{\partial y^2}&=\sin^2\theta\frac{\partial^2}{\partial r^2}+\frac{\sin 2\theta}{r}\frac{\partial^2}{\partial r\partial\theta}+\frac{\cos^2\theta}{r}\frac{\partial}{\partial r}-\frac{\sin 2\theta}{r^2}\frac{\partial}{\partial\theta}+\frac{\cos^2\theta}{r^2}\frac{\partial^2}{\partial\theta^2}\\\frac{\partial^2}{\partial x\partial y}&=\frac{\sin 2\theta}{2}\frac{\partial^2}{\partial r^2}+\frac{\cos 2\theta}{r}\frac{\partial^2}{\partial r\partial\theta}-\frac{\sin 2\theta}{2r}\frac{\partial}{\partial r}-\frac{\cos 2\theta}{r^2}\frac{\partial}{\partial\theta}-\frac{\sin 2\theta}{2r^2}\frac{\partial^2}{\partial\theta^2}\end{aligned}\tag{20}$$

where Δ is the area of the triangular element, and,

$$\mathbf{T}=\begin{bmatrix} b_1^2 & b_2^2 & 2b_1b_2 \\ c_1^2 & c_2^2 & 2c_1c_2 \\ 2b_1c_1 & 2b_2c_2 & 2(b_1c_2+b_2c_1) \end{bmatrix}.$$

According to Eqs. (7) and (14)-(20), the strains of element can be obtained:

$$\varepsilon=-z\mathbf{B}\delta \tag{21}$$

where,

$$\delta=[\mathbf{u}_1 \quad \mathbf{u}_2 \quad \mathbf{u}_3 \quad \mathbf{u}_4]^{\mathrm{T}},$$
$$\mathbf{u}_1=\{w_1,\theta_{x1},\theta_{y1},w_2,\theta_{x2},\theta_{y2},w_3,\theta_{x3},\theta_{y3}\},$$
$$\mathbf{u}_2=[\mathbf{u}_{21} \quad \mathbf{u}_{22} \quad \mathbf{u}_{23}],$$
$$\mathbf{u}_{2k}=\{a_k^1,a_k^2,\cdots,a_k^{16},b_k^1,b_k^2,\cdots,b_k^{16},c_k^1,c_k^2,\cdots,c_k^{16}\}$$

and,

$$(k=1,2,3),$$
$$\mathbf{u}_3=\{d_1,d_2,d_3\},$$
$$\mathbf{u}_4=\{e_1,e_2,e_3\},$$
$$\mathbf{B}=[\mathbf{B_1} \quad \mathbf{B_2} \quad \mathbf{B_3} \quad \mathbf{B_4}],$$
$$\mathbf{B_1}=\frac{1}{4\Delta^2}\mathbf{T}\begin{bmatrix} \mathbf{N}_{1,11} & \mathbf{N}_{2,11} & \mathbf{N}_{3,11} \\ \mathbf{N}_{1,22} & \mathbf{N}_{2,22} & \mathbf{N}_{3,22} \\ \mathbf{N}_{1,12} & \mathbf{N}_{2,12} & \mathbf{N}_{3,12} \end{bmatrix}$$

where the notations like $\mathbf{N}_{1,11}$ represent the second partial derivatives of the shape function $\mathbf{N}_1$ with respect to the area coordinate L_1. In addition, $\mathbf{B}_2=[\mathbf{B}_{21} \quad \mathbf{B}_{22} \quad \mathbf{B}_{23}]$, $\mathbf{B}_{2k}=\{\mathbf{\Lambda}_k^1,\mathbf{\Lambda}_k^2,\cdots,\mathbf{\Lambda}_k^{16},\mathbf{\Lambda}_{xk}^1,\mathbf{\Lambda}_{xk}^2,\cdots,\mathbf{\Lambda}_{xk}^{16},\mathbf{\Lambda}_{yk}^1,\mathbf{\Lambda}_{yk}^2,\cdots,\mathbf{\Lambda}_{yk}^{16}\}$, $(k=1,2,3)$, where,

$$\mathbf{\Lambda}_k^j=\frac{1}{4\mathbf{\Delta}^2}\mathbf{T}\begin{Bmatrix} N_{k,11} \\ N_{k,22} \\ N_{k,12} \end{Bmatrix}\left(F^j-F_k^j\right)+\frac{1}{\mathbf{\Delta}}\begin{bmatrix} \lambda_a^jb_1 & \lambda_a^jb_2 \\ \eta_a^jc_1 & \eta_a^jc_2 \\ \eta_a^jb_1+\lambda_a^jc_1 & \eta_a^jb_2+\lambda_a^jc_2 \end{bmatrix}\begin{Bmatrix} N_{k,1} \\ N_{k,2} \end{Bmatrix}+\begin{Bmatrix} F_{,xx}^j \\ F_{,yy}^j \\ 2F_{,xy}^j \end{Bmatrix}N_k,$$

$$\mathbf{\Lambda}_{xk}^j=\frac{1}{4\mathbf{\Delta}^2}\mathbf{T}\begin{Bmatrix} N_{xk,11} \\ N_{xk,22} \\ N_{xk,12} \end{Bmatrix}\left(F_x^j-F_{xk}^j\right)+\frac{1}{\mathbf{\Delta}}\begin{bmatrix} \lambda_b^jb_1 & \lambda_b^jb_2 \\ \eta_b^jc_1 & \eta_b^jc_2 \\ \eta_b^jb_1+\lambda_b^jc_1 & \eta_b^jb_2+\lambda_b^jc_2 \end{bmatrix}\begin{Bmatrix} N_{xk,1} \\ N_{xk,2} \end{Bmatrix}+\begin{Bmatrix} F_{x,xx}^j \\ F_{x,yy}^j \\ 2F_{x,xy}^j \end{Bmatrix}N_{xk},$$

$$\mathbf{\Lambda}_{yk}^j=\frac{1}{4\mathbf{\Delta}^2}\mathbf{T}\begin{Bmatrix} N_{yk,11} \\ N_{yk,22} \\ N_{yk,12} \end{Bmatrix}\left(F_y^j-F_{yk}^j\right)+\frac{1}{\mathbf{\Delta}}\begin{bmatrix} \lambda_c^jb_1 & \lambda_c^jb_2 \\ \eta_c^jc_1 & \eta_c^jc_2 \\ \eta_c^jb_1+\lambda_c^jc_1 & \eta_c^jb_2+\lambda_c^jc_2 \end{bmatrix}\begin{Bmatrix} N_{yk,1} \\ N_{yk,2} \end{Bmatrix}+\begin{Bmatrix} F_{y,xx}^j \\ F_{y,yy}^j \\ 2F_{y,xy}^j \end{Bmatrix}N_{yk},$$

in which,

$$\lambda_a^j=\frac{\partial F^j}{\partial r}\cos\theta-\frac{\partial F^j}{\partial\theta}\frac{\sin\theta}{r},\ \eta_a^j=\frac{\partial F^j}{\partial r}\sin\theta+\frac{\partial F^j}{\partial\theta}\frac{\cos\theta}{r},\ \lambda_b^j=\frac{\partial F_x^j}{\partial r}\cos\theta-\frac{\partial F_x^j}{\partial\theta}\frac{\sin\theta}{r},$$
$$\eta_b^j=\frac{\partial F_x^j}{\partial r}\sin\theta+\frac{\partial F_x^j}{\partial\theta}\frac{\cos\theta}{r},\ \lambda_c^j=\frac{\partial F_y^j}{\partial r}\cos\theta-\frac{\partial F_y^j}{\partial\theta}\frac{\sin\theta}{r},\ \eta_c^j=\frac{\partial F_y^j}{\partial r}\sin\theta+\frac{\partial F_y^j}{\partial\theta}\frac{\cos\theta}{r},\ (j=1,2,3,\cdots,16).$$

In the expressions above, the derivatives of the enrichment function with respect to Cartesian coordinates are transformed to polar coordinates via Eq. (20). Furthermore,

$$\mathbf{B}_3=\frac{1}{4\Delta^2}\mathbf{T}\begin{bmatrix} N_{1,11}[H(\mathbf{x})-H(\mathbf{x}_1)] & N_{2,11}[H(\mathbf{x})-H(\mathbf{x}_2)] & N_{3,11}[H(\mathbf{x})-H(\mathbf{x}_3)] \\ N_{1,22}[H(\mathbf{x})-H(\mathbf{x}_1)] & N_{2,22}[H(\mathbf{x})-H(\mathbf{x}_2)] & N_{3,22}[H(\mathbf{x})-H(\mathbf{x}_3)] \\ N_{1,12}[H(\mathbf{x})-H(\mathbf{x}_1)] & N_{2,12}[H(\mathbf{x})-H(\mathbf{x}_2)] & N_{3,12}[H(\mathbf{x})-H(\mathbf{x}_3)] \end{bmatrix}$$

and $\mathbf{B}_4=[\mathbf{B}_{41} \quad \mathbf{B}_{42} \quad \mathbf{B}_{43}]$, where,

$$\mathbf{B}_{4k}=\frac{1}{4\Delta^2}\mathbf{T}\begin{Bmatrix} N_{k,11} \\ N_{k,22} \\ N_{k,12} \end{Bmatrix}S(x)+\frac{1}{\Delta}\begin{bmatrix} b_1N_{k,1}+b_2N_{k,2} & 0 \\ 0 & c_1N_{k,1}+c_2N_{k,2} \\ c_1N_{k,1}+c_2N_{k,2} & b_1N_{k,1}+b_2N_{k,2} \end{bmatrix}\begin{Bmatrix} S(x)_{,x} \\ S(x)_{,y} \end{Bmatrix}+N_k\begin{Bmatrix} S(x)_{,xx} \\ S(x)_{,yy} \\ 2S(x)_{,xy} \end{Bmatrix},$$

and,

$$\begin{Bmatrix} S(x)_{,x} \\ S(x)_{,y} \end{Bmatrix}=\sum_{i=1}^{3}\frac{1}{2\Delta}\begin{bmatrix} b_1 & b_2 \\ c_1 & c_2 \end{bmatrix}\begin{Bmatrix} N_{i,1} \\ N_{i,2} \end{Bmatrix}|\phi_i|-\left|\sum_{i=1}^{3}\frac{1}{2\Delta}\begin{bmatrix} b_1 & b_2 \\ c_1 & c_2 \end{bmatrix}\begin{Bmatrix} N_{i,1} \\ N_{i,2} \end{Bmatrix}\phi_i\right|,\quad \begin{Bmatrix} S(x)_{,xx} \\ S(x)_{,yy} \\ 2S(x)_{,xy} \end{Bmatrix}=\sum_{i=1}^{3}\frac{1}{4\Delta^2}\mathbf{T}\begin{Bmatrix} N_{i,11} \\ N_{i,22} \\ N_{i,12} \end{Bmatrix}|\phi_i|-\left|\sum_{i=1}^{3}\frac{1}{4\Delta^2}\mathbf{T}\begin{Bmatrix} N_{i,11} \\ N_{i,22} \\ N_{i,12} \end{Bmatrix}\phi_i\right|.$$

In the element domain V_e, the total potential energy is:

$$\Pi = \int_{V_e} \left(\frac{1}{2} \varepsilon^{\mathrm{T}} \sigma - qw \right) dV \tag{22}$$

According to the principle of minimum potential energy $\delta\Pi = 0$, the element formulation for the extended finite element analysis can be obtained:

$$\mathbf{K}_e \, \boldsymbol{\delta} = \mathbf{P} \tag{23}$$

where $\mathbf{K}_e = \mathbf{B}^{\mathrm{T}} \mathbf{D} \mathbf{B}$ is the element stiffness matrix and $\mathbf{P}$ is the equivalent nodal load vector,

$$\mathbf{P} = \{\mathbf{P}_1, \mathbf{P}_2, \mathbf{P}_3, \mathbf{P}_4\}^{\mathrm{T}} \tag{24}$$

where $\mathbf{P}_1 = \int_{V_e} \mathbf{N}^{\mathrm{T}} q dV$, $\mathbf{P}_2 = \int_{V_e} [\mathbf{P}_{21} \quad \mathbf{P}_{22} \quad \mathbf{P}_{23}]^{\mathrm{T}} q dV$, and,

$$\begin{aligned} \mathbf{P}_{2k} = \{ & N_k \left(F^1 - F_k^1 \right), N_k \left(F^2 - F_k^2 \right), \cdots, N_k \left(F^{16} - F_k^{16} \right), \\ & N_{xk} \left(F_x^1 - F_{xk}^1 \right), N_{xk} \left(F_x^2 - F_{xk}^2 \right), \cdots, N_{xk} \left(F_x^{16} - F_{xk}^{16} \right), \\ & N_{yk} \left(F_y^1 - F_{yk}^1 \right), N_{yk} \left(F_y^2 - F_{yk}^2 \right), \cdots, N_{yk} \left(F_y^{16} - F_{yk}^{16} \right) \}, \quad (k = 1,2,3) \end{aligned}$$

$$\mathbf{P}_3 = \int_{V_e} \left\{ N_1 [H(\mathbf{x}) - H(\mathbf{x}_1)], N_2 [H(\mathbf{x}) - H(\mathbf{x}_2)], N_3 [H(\mathbf{x}) - H(\mathbf{x}_3)] \right\}^{\mathrm{T}} q dV,$$

$$\mathbf{P}_4 = \int_{V_e} \left\{ N_1 S(\mathbf{x}), N_2 S(\mathbf{x}), N_3 S(\mathbf{x}) \right\}^{\mathrm{T}} q dV.$$

4. Interaction Integral

As indicated in Eq. (6), the stresses reach their maximum values on the upper and lower surfaces during plate bending deformation. Therefore, in strength evaluation, these surfaces, corresponding to z = h/2, are selected for analysis. Two stress states are considered on the plate surface: State I represents the actual field, whose physical quantities are computed using the XFEM; State II denotes the auxiliary field, derived from the symplectic analytical solution. The contour interaction energy integral is then defined as follows:

$$U = \int_{\Gamma} \left(\sigma_{ik}^{\mathrm{I}} \varepsilon_{ik}^{\mathrm{II}} \delta_{xj} - \sigma_{ij}^{\mathrm{I}} u_{i,x}^{\mathrm{II}} - \sigma_{ij}^{\mathrm{II}} u_{i,x}^{\mathrm{I}} \right) q n_j \mathrm{d}\Gamma, \quad (i,j,k = x,y) \tag{25}$$

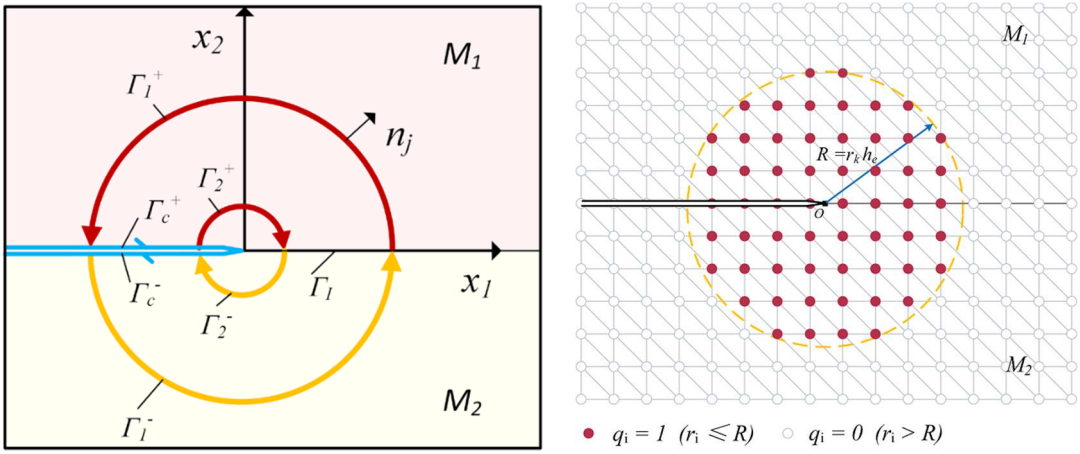
In the above expression, Γ represents a contour enclosing the crack tip, extending from the lower crack surface to the upper crack surface. The quantities $\sigma_{ij}^{\mathrm{I}}, \varepsilon_{ij}^{\mathrm{I}}, u_i^{\mathrm{I}}$ denote the stress, strain, and displacement components of the actual field on the plate surface, respectively; $\sigma_{ij}^{\mathrm{II}}, \varepsilon_{ij}^{\mathrm{II}}, u_i^{\mathrm{II}}$ refer to those of the auxiliary field. Here, δ_{ij} is the Kronecker delta, q is a weight function, and n_j is the unit outward normal vector to the contour Γ. The contour, i.e., the integration path, is illustrated in Fig. 2(a) and can be expressed as:

$$\Gamma = \Gamma_c^- + \Gamma_1^- + \Gamma_1^+ + \Gamma_c^+ + \Gamma_2^+ + \Gamma_2^- \tag{26}$$

The contour form of the interaction integral can be converted into a domain form using the divergence theorem [33], and the converted form is:

$$U = \int_{A} \left(\sigma_{ik}^{\mathrm{I}} \varepsilon_{ik}^{\mathrm{II}} \delta_{xj} - \sigma_{ij}^{\mathrm{I}} u_{i,x}^{\mathrm{II}} - \sigma_{ij}^{\mathrm{II}} u_{i,x}^{\mathrm{I}} \right) q_{,j} \mathrm{d}A, \quad (i,j,k = x,y) \tag{27}$$

where A denotes a circular domain centered at the crack tip with radius R.



(a) (b)

Fig. 2. (a) Integration contours of the interaction integral around a bi-material interfacial crack tip; (b) Nodal assignment of the weight function in the domain form of the interaction integral.

In finite element implementation, the integration domain radius is defined as $R = r_k h_e$, where r_k is a user-specified scalar multiple [34], and h_e represents the characteristic size of the crack-tip element. The weight function q is assigned a value of 1 for nodes inside A, and 0 for nodes outside A, as shown in Fig. 2(b). Within an element, the weight function can be interpolated from nodal values using shape functions of the three-node triangular element:

$$q = \sum_{i=1}^{3} L_i q_i \tag{28}$$

Here, L_i is given by Eq. (10). The relationship between the interaction integral and the SIFs [35] is as follows:

$$U = \frac{2}{E^* \cosh^2(\pi s)}\left(K_1 K_1^{II} + K_2 K_2^{II}\right) \tag{29}$$

where K_1^{II} and K_2^{II} are auxiliary stress intensity factors for the auxiliary fields, K_1 and K_2 denote the mode I and mode II SIFs at the crack tip in the actual field, respectively, $E^* = 2E^{(1)}E^{(2)}/(E^{(1)} + E^{(2)})$. By setting $K_1^{II} = 1$ and $K_2^{II} = 0$, K_1 can be calculated by $K_1 = UE^* \cosh^2(\pi s)/2$; similarly, $K_2 = UE^* \cosh^2(\pi s)/2$ can be calculated by setting $K_1^{II} = 0$ and $K_2^{II} = 1$.

The displacement, stress, and strain of the auxiliary field on the plate surface under bending can be derived from the symplectic series terms with eigenvalues less than 1, as given in Eq. (8). For Material 1, substitute the eigenvalues $\mu_1 = 0.5 - si$ and $\mu_2 = 0.5 + si$ into Eq. (A2). At this time, $\det(\gamma) = 0$, setting $C^{(1)} = 1$ yields:

$$\begin{aligned} A_1^{(1)} &= -\frac{\zeta_4 + 1}{\zeta_2 - 1} \\ B_1^{(1)} &= \frac{(\zeta_4 + 1 + \zeta_1\zeta_2 - \zeta_1)(\zeta_3 - \zeta_1)}{(\zeta_1\zeta_2 - \zeta_3)(\zeta_2 - 1)} \frac{e^{s\pi} - e^{-s\pi}}{e^{s\pi} + e^{-s\pi}} \mathrm{i} \\ G_1^{(1)} &= \frac{\zeta_4 + 1 + \zeta_1\zeta_2 - \zeta_1}{\zeta_3 - \zeta_1\zeta_2} \frac{e^{s\pi} - e^{-s\pi}}{e^{s\pi} + e^{-s\pi}} \mathrm{i} \end{aligned} \tag{30}$$

$$\begin{aligned} A_2^{(1)} &= A_1^{(1)} \\ B_2^{(1)} &= -B_1^{(1)} \\ G_2^{(1)} &= -G_1^{(1)} \end{aligned} \tag{31}$$

where A and B are complex numbers, G is a pure imaginary number. Substituting these into Eq. (8) gives the plate deflection:

$$w^{(1)} = w_1^{(1)} + w_2^{(1)} \tag{32}$$

where,

$$\begin{aligned} w_i^{(1)} = {} & \frac{1}{2D} r^{\frac{3}{2}} \cos(s \ln r)\left[\frac{6\varphi_i}{(9+4s^2)(1-\upsilon)} - \frac{4s\varphi_i'}{(9+4s^2)(1-\upsilon)} - \frac{(14+2\upsilon)\bar{\varphi}_i}{(7+\upsilon)^2 + 4s^2(1-\upsilon)^2} - \frac{4s(1-\upsilon)\hat{\varphi}_i}{(7+\upsilon)^2 + 4s^2(1-\upsilon)^2}\right] \\ & + \frac{1}{2D} r^{\frac{3}{2}} \sin(s \ln r)\left[\frac{6\varphi_i'}{(9+4s^2)(1-\upsilon)} + \frac{4s\varphi_i}{(9+4s^2)(1-\upsilon)} + \frac{(14+2\upsilon)\hat{\varphi}_i}{(7+\upsilon)^2 + 4s^2(1-\upsilon)^2} - \frac{4s(1-\upsilon)\bar{\varphi}_i}{(7+\upsilon)^2 + 4s^2(1-\upsilon)^2}\right], (i = 1,2) \end{aligned} \tag{33}$$

and,

$$\varphi_1 = \left[\mathrm{Re}\left(A_1^{(1)}\right)\eta_1 + \mathrm{Im}(B_1^{(1)})\eta_2\right]\cos\left(\frac{3\theta}{2}\right) + \left[\mathrm{Im}\left(A_1^{(1)}\right)\eta_2 - \mathrm{Re}\left(B_1^{(1)}\right)\eta_1\right]\sin\left(\frac{3\theta}{2}\right),$$

$$\varphi_1' = \left[\mathrm{Re}\left(A_1^{(1)}\right)\eta_2 + \mathrm{Im}\left(B_1^{(1)}\right)\eta_1\right]\sin\left(\frac{3\theta}{2}\right) - \left[\mathrm{Im}\left(A_1^{(1)}\right)\eta_1 - \mathrm{Re}\left(B_1^{(1)}\right)\eta_2\right]\cos\left(\frac{3\theta}{2}\right),$$

$$\bar{\varphi}_1 = \eta_1 \cos\left(\frac{\theta}{2}\right) - \mathrm{Im}\left(G_1^{(1)}\right)\eta_2 \cos\left(\frac{\theta}{2}\right),$$

$$\hat{\varphi}_1 = \eta_2 \sin\left(\frac{\theta}{2}\right) - \mathrm{Im}\left(G_1^{(1)}\right)\eta_1 \sin\left(\frac{\theta}{2}\right),$$

$$\varphi_2 = \left[\mathrm{Re}\left(A_1^{(1)}\right)\eta_1 + \mathrm{Im}\left(B_1^{(1)}\right)\eta_2\right]\cos\left(\frac{3\theta}{2}\right) - \left[\mathrm{Im}\left(A_1^{(1)}\right)\eta_2 - \mathrm{Re}\left(B_1^{(1)}\right)\eta_1\right]\sin\left(\frac{3\theta}{2}\right),$$

$$\varphi_2' = \left[\mathrm{Re}\left(A_1^{(1)}\right)\eta_2 + \mathrm{Im}\left(B_1^{(1)}\right)\eta_1\right]\sin\left(\frac{3\theta}{2}\right) + \left[\mathrm{Im}\left(A_1^{(1)}\right)\eta_1 - \mathrm{Re}\left(B_1^{(1)}\right)\eta_2\right]\cos\left(\frac{3\theta}{2}\right),$$

$$\bar{\varphi}_2 = \bar{\varphi}_1, \quad \hat{\varphi}_2 = \hat{\varphi}_1, \quad \eta_1 = e^{s\theta} + e^{-s\theta}, \quad \eta_2 = e^{s\theta} - e^{-s\theta}.$$

The coefficients in the symplectic analytical solution for Material 2 are calculated using Eq. (A1) and substituted into Eq. (8) to obtain the deflection of Material 2.

According to the relationship between displacement and deflection in Kirchhoff theory, the displacements of the auxiliary field on the plate surface are:

$$u_x^{II} = \frac{h}{2}\left(\frac{1}{r}\frac{\partial w}{\partial \theta}\sin\theta - \frac{\partial w}{\partial r}\cos\theta\right), \quad u_y^{II} = -\frac{h}{2}\left(\frac{\partial w}{\partial r}\sin\theta + \frac{1}{r}\frac{\partial w}{\partial \theta}\cos\theta\right), \tag{34}$$

The stress and strain in the auxiliary field are computed using Eq. (6) and Eq. (7), respectively. In this formulation, the partial derivatives of the deflection with respect to Cartesian coordinates are transformed to polar coordinates via Eq. (20).

5. Numerical Examples

5.1. A square plate with a central interface crack subjected to bending moment

As shown in Fig. 3(a), a rectangular plate of dimensions $H \times W$ and thickness h contains a central interface crack of length a inclined at an angle α. The XFEM mesh is shown in Fig. 3(b). The red solid line indicates the crack location, and the green solid line indicates the material interface. Red asterisks denote crack-face enriched nodes, red circles denote crack-tip enriched nodes, and red squares denote material-interface enriched nodes. For the square configuration where $H = W$, bending moments M are applied to the upper and lower boundaries as shown in Fig. 3(c), the Poisson's ratios are set to $\upsilon_1 = \upsilon_2 = 0.3$, the normalized SIFs K_1 and K_2 are calculated for varying crack lengths, elastic modulus ratios between the two materials, and crack inclination angles. The results are summarized in Tables 1 and 2, where the normalization factor is $M\sqrt{\pi a/2}/h^2$. The numerical results indicate that as the material properties on both sides of the interface approach each other, the stress intensity factors converge to those reported for a homogeneous plate under bending [36]. Although the methods employed for solving the stress intensity factor differ from those in existing literature [3, 36, 37], all approaches define the SIFs as the coefficients of the singular term in the crack-tip stress field. As shown in Tables 1 and 2, both K_1 and K_2 increase with increasing crack length. With increasing inclination angle α, K_1 decreases while K_2 increases, which is consistent with the variation trend observed in homogeneous plates. Moreover, K_1 decreases with a higher elastic modulus ratio, whereas K_2 increases. For clarity, the variation of the SIFs with the structural parameters is plotted in Figs. 4 and 5. In addition, for a crack inclination angle of 0° and Poisson's ratios of $\upsilon_1 = \upsilon_2 = 0.3$, a comparison between the results obtained using the present method and those reported in Ref. [21] is presented in Fig. 6. The results show good agreement with those reported in the literature. It should be noted that the normalization factor of the SIFs in Ref. [21] differs from that in the present study by a $\sqrt{\pi}$ term. Furthermore, for the specific case of $E_1 : E_2 = 2:1$ and a crack inclination angle of 0°, Table 3 presents the SIFs for different Poisson's ratios and crack lengths. The corresponding variation of SIFs is shown in Fig. 7. The data suggest that Poisson's ratio exerts a more pronounced influence on K_2 than on K_1. A mesh convergence study is then performed with $E_1 : E_2 = 2:1$, crack inclination angle of 0°, $\upsilon_1 = \upsilon_2 = 0.3$, and $a/W = 0.2$. Figure 8 shows the variation of the normalized SIFs K_1 and K_2 with the number of nodes, demonstrating good mesh convergence of the present method. In addition, Table 4 presents the computed SIFs for different values of the user-specified scalar multiple r_k. As shown in the table, the results tend to converge when $r_k \geq 5$. Therefore, $r_k = 6$ is adopted in all numerical examples in this study.

5.2. A rectangular plate with a central interface crack under transverse load

As shown in Fig. 3(d), a bi-material rectangular plate with a central interface crack is considered. The plate is simply supported on all four sides and subjected to a uniform transverse pressure q_0. The aspect ratio of the plate is H:W = 1.2:1. For Poisson's ratios of $\upsilon_1 = \upsilon_2 = 0.3$, the normalized SIFs for various crack inclination angles, elastic modulus ratios, and crack lengths are presented in Tables 5 and 6. Here, the normalization parameter is $q_0 W^2 \sqrt{\pi a/2}/h^2$. Both K_1 and K_2 decrease with increasing crack length, though the variation in K_2 is significantly less pronounced than that in K_1. Moreover, K_1 decreases as the elastic modulus ratio increases, whereas K_2 shows an opposite trend. These results indicate that a higher elastic modulus mismatch tends to suppress Mode I fracture while promoting Mode II fracture. When the crack inclination angle is 0° and the elastic moduli of the two materials approach each other, the calculated stress intensity factors agree well with the values reported in the literature [36]. The variation of the stress intensity factor with the structural parameters is illustrated in Figs. 9 and 10.

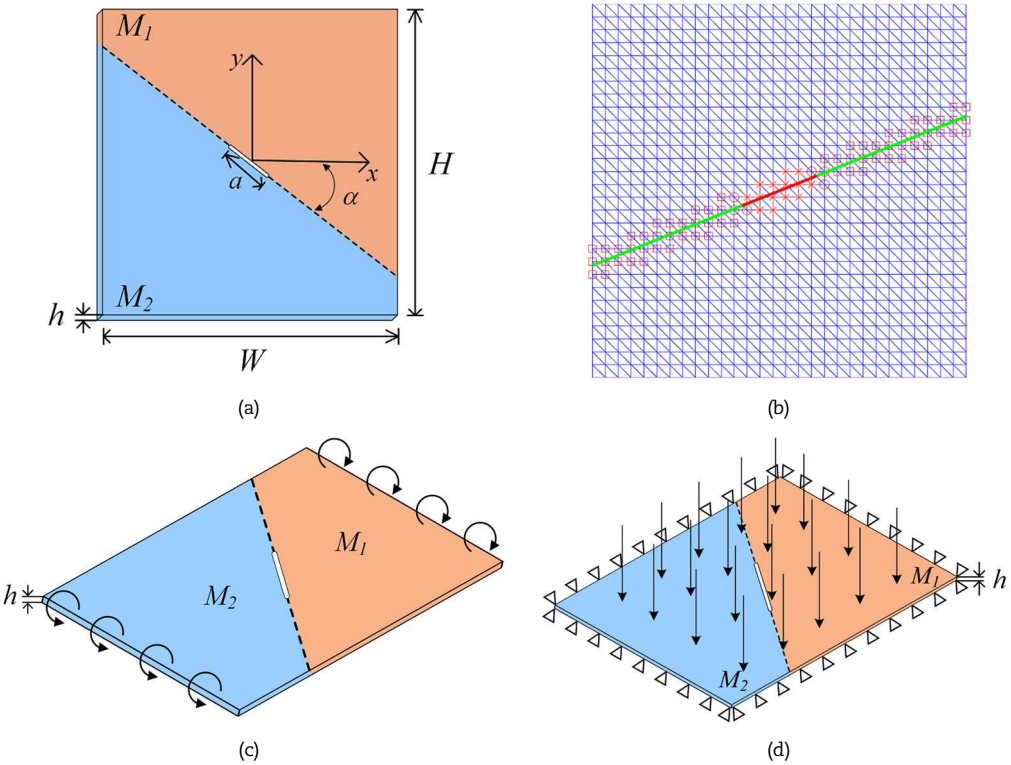


Fig. 3. (a) Rectangular plate with a central crack; (b) DKT mesh and distribution of enriched nodes for a plate with an interface crack; (c) Square plate with a central crack under bending moment; (d) Simply supported rectangular plate with a central interface crack under uniform loads.

Table 1. Normalized SIFs K_1 for square plates containing central interface cracks at various inclination angles under bending moments.

	E_1:E_2	a/W						
		0.2	0.3	0.4	0.5	0.6	0.7	0.8
$\alpha = 45°$	10:1	1.8884	1.9023	1.9709	2.0726	2.2158	2.3984	2.6163
	5:1	2.0555	2.0838	2.1570	2.2598	2.4183	2.6246	2.8733
	2:1	2.6117	2.6365	2.7461	2.8928	3.1034	3.3980	3.7562
$\alpha = 30°$	10:1	2.4875	2.5085	2.6113	2.7338	3.0012	3.3125	3.6994
	5:1	2.7382	2.7506	2.8605	3.0146	3.2724	3.5919	4.0199
	2:1	3.5425	3.5899	3.7442	3.9541	4.2680	4.7219	5.2692
$\alpha = 15°$	10:1	2.9738	3.0156	3.1465	3.2790	3.6316	3.9928	4.4801
	5:1	3.2844	3.3099	3.4365	3.6383	3.9246	4.3095	4.8117
	2:1	4.2849	4.3515	4.5558	4.7823	5.2038	5.7722	6.4406
$\alpha = 0°$	10:1	3.1967	3.2246	3.3617	3.5251	3.8816	4.1967	4.7125
	5:1	3.5309	3.5475	3.6940	3.8995	4.2165	4.6292	5.1465
	2:1	4.6033	4.6532	4.8722	5.1255	5.5667	6.1759	6.8923
	1.01:1	6.0651	6.1867	6.4156	6.7628	7.1974	7.8741	8.9672
	Homog. Plate Ref. [36]	6.1042	6.2448	6.4603	6.7767	7.2434	7.9625	9.1624

Table 2. Normalized SIFs K_2 for square plates containing central interface cracks at various inclination angles under bending moments.

	E_1:E_2	a/W						
		0.2	0.3	0.4	0.5	0.6	0.7	0.8
$\alpha = 45°$	10:1	4.1764	4.4152	4.7368	5.2830	5.8450	6.4952	7.1834
	5:1	3.9063	4.0524	4.2970	4.7118	5.1214	5.5674	6.0914
	2:1	3.5850	3.6856	3.8352	3.9950	4.1712	4.4542	4.6968
$\alpha = 30°$	10:1	3.6112	3.8409	4.1740	4.6124	5.0764	5.6595	6.2928
	5:1	3.3774	3.5440	3.7932	4.0977	4.4698	4.8733	5.2898
	2:1	3.1013	3.2264	3.3359	3.4916	3.6842	3.8547	4.1194
$\alpha = 15°$	10:1	2.0982	2.2176	2.3984	2.6515	2.9425	3.2676	3.6217
	5:1	1.9615	2.0462	2.1785	2.3659	2.5807	2.8137	3.0657
	2:1	1.8025	1.8628	1.9376	2.0275	2.1156	2.2371	2.3784
$\alpha = 0°$	10:1	1.0126	1.1104	1.2758	1.4437	1.6524	1.8781	2.2129
	5:1	0.7376	0.8183	0.9227	1.0537	1.1789	1.3295	1.5481
	2:1	0.4642	0.5127	0.5669	0.6435	0.7224	0.8312	0.9421
	1.01:1	0.0113	0.0222	0.0263	0.0358	0.0649	0.1152	0.1729
	Homog. Plate Ref. [36]	-0.00024	-0.00028	-0.00025	-0.00017	-0.00056	-0.000001	-0.00018

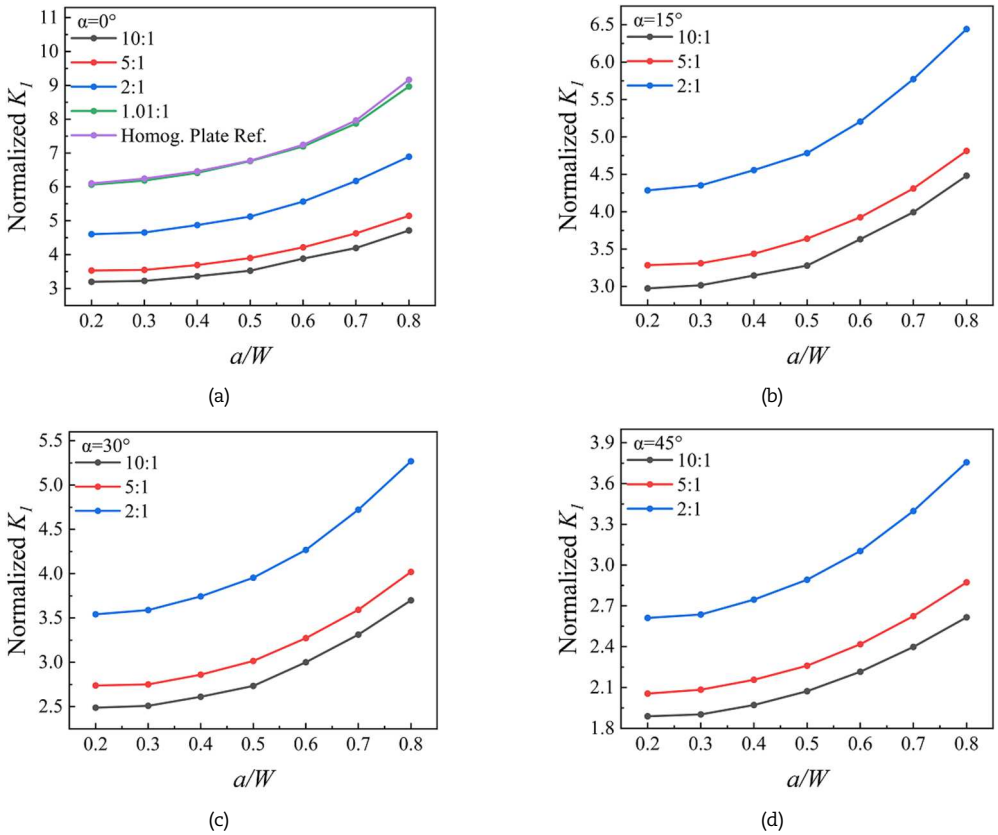


Fig. 4. Normalized SIFs K_1 for square plates containing central interface cracks at various inclination angles under bending moments: (a) $\alpha = 0°$; (b) $\alpha = 15°$; (c) $\alpha = 30°$; (d) $\alpha = 45°$.

Table 3. Normalized SIFs of square plates with central interface cracks under bending moment for different Poisson's ratios and crack lengths.

	υ_1, υ_2	a/W						
		0.2	0.3	0.4	0.5	0.6	0.7	0.8
K_1	0.3,0.1	4.1635	4.2485	4.4217	4.6531	4.9831	5.3770	5.8572
	0.3,0.2	4.3586	4.4580	4.6363	4.8624	5.2193	5.6598	6.1617
	0.3,0.4	4.7888	4.8768	5.0670	5.3255	5.7726	6.3070	6.9483
K_2	0.3,0.1	0.2112	0.2236	0.2407	0.2561	0.2781	0.3105	0.3657
	0.3,0.2	0.3314	0.3497	0.3912	0.4374	0.5036	0.5947	0.7026
	0.3,0.4	0.6188	0.6762	0.7613	0.8612	1.0033	1.1854	1.4102

Table 4. Effect of the integration domain radius on the normalized SIFs.

r_k	2	3	4	5	6	7	8
K_1	4.7824	4.7051	4.6385	4.6033	4.6067	4.6112	4.6130
K_2	0.4751	0.4686	0.4657	0.4648	0.4642	0.4641	0.4641

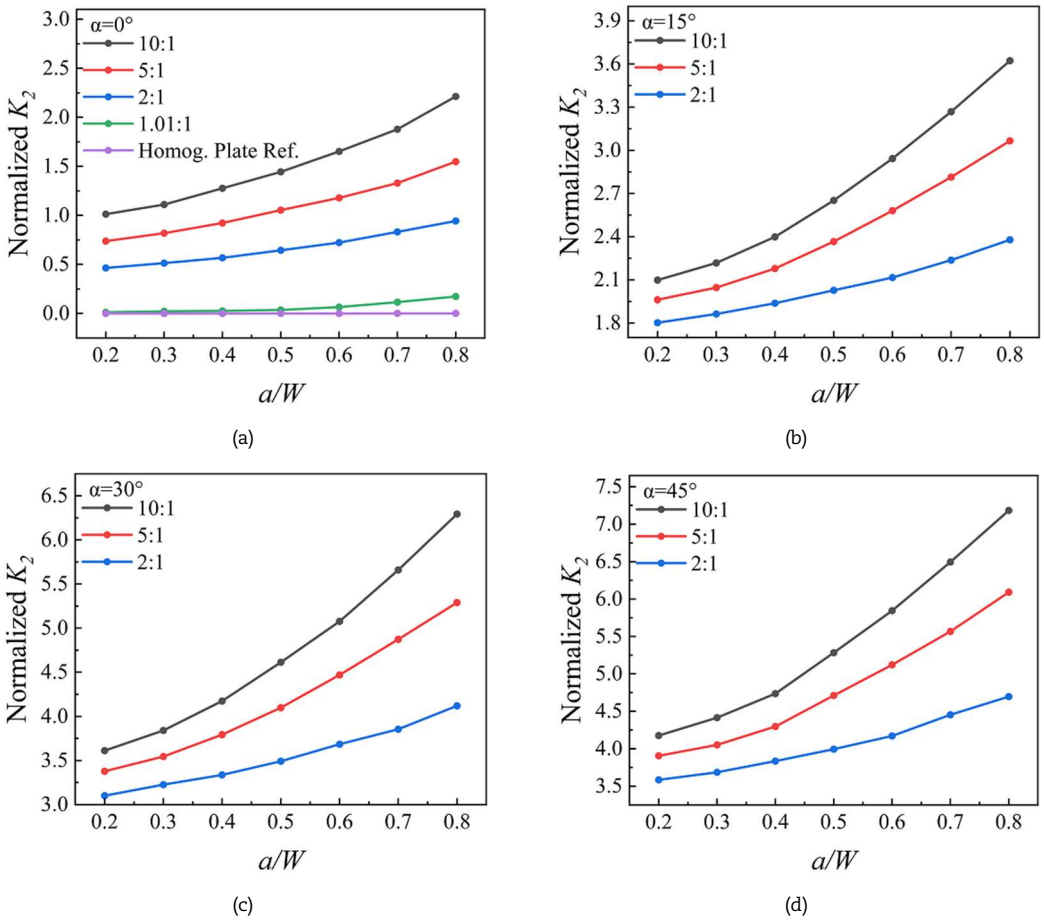


Fig. 5. Normalized SIFs K_2 for square plates containing central interface cracks at various inclination angles under bending moments: (a) $\alpha = 0°$; (b) $\alpha = 15°$; (c) $\alpha = 30°$; (d) $\alpha = 45°$.

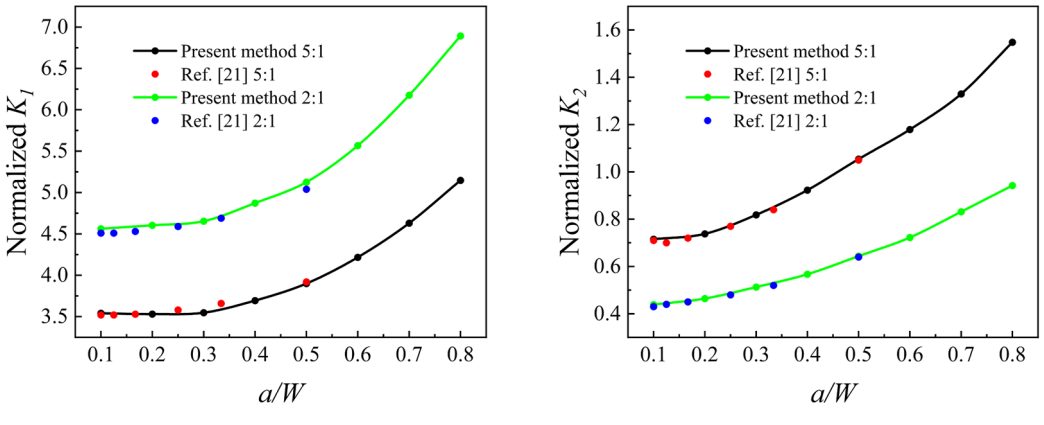


Fig. 6. Comparison of normalized SIFs between the present method and Ref. [21]: (a) K_1; (b) K_2.

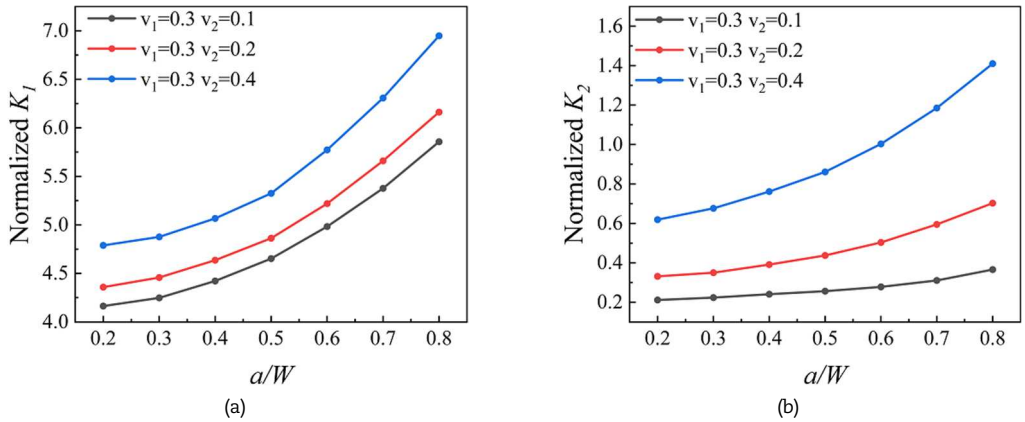


Fig. 7. Normalized SIFs for square plates containing central interface cracks at various Poisson's ratios and crack lengths under bending moment: (a) K_1; (b) K_2.

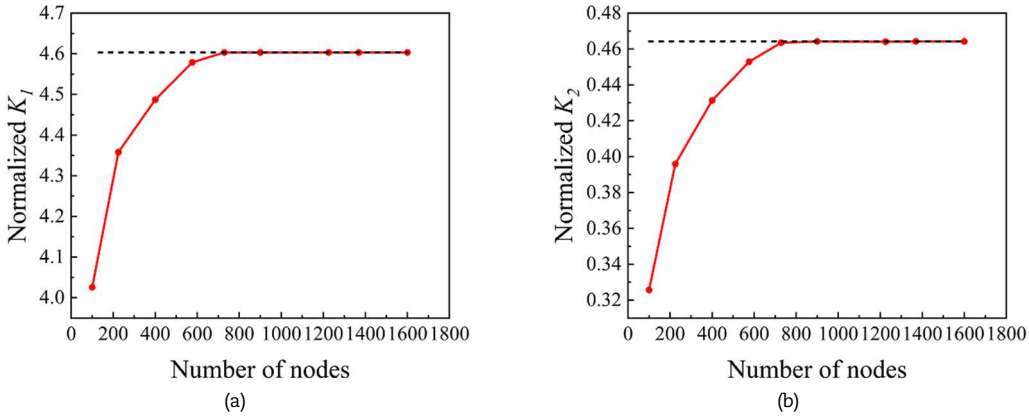


Fig. 8. Mesh convergence of the normalized SIFs for a bi-material interface crack: (a) K_1; (b) K_2.

Table 5. Normalized SIFs K_1 for rectangular plates containing central interface cracks at various inclination angles under uniform load.

	E_1:E_2	a/W						
		0.2	0.3	0.4	0.5	0.6	0.7	0.8
$\alpha = 45°$	10:1	0.1817	0.1727	0.1683	0.1519	0.1433	0.1204	0.0970
	5:1	0.2107	0.2014	0.1859	0.1802	0.1579	0.1362	0.1071
	2:1	0.2663	0.2530	0.2375	0.2207	0.2000	0.1723	0.1337
$\alpha = 30°$	10:1	0.1796	0.1740	0.1675	0.1577	0.1377	0.1214	0.0975
	5:1	0.2095	0.2015	0.1878	0.1765	0.1569	0.1340	0.1028
	2:1	0.2639	0.2544	0.2392	0.2219	0.2021	0.1736	0.1346
$\alpha = 15°$	10:1	0.1816	0.1765	0.1705	0.1546	0.1473	0.1201	0.0973
	5:1	0.2065	0.1995	0.1919	0.1788	0.1649	0.1347	0.1058
	2:1	0.2682	0.2561	0.2421	0.2248	0.2036	0.1739	0.1364
$\alpha = 0°$	10:1	0.1926	0.1835	0.1708	0.1591	0.1493	0.1252	0.0962
	5:1	0.2136	0.2037	0.1914	0.1802	0.1650	0.1463	0.1089
	2:1	0.2689	0.2592	0.2462	0.2285	0.2087	0.1782	0.1387
	1.01:1	0.3423	0.3247	0.3082	0.2862	0.2616	0.2234	0.1739
	Homog. Plate Ref. [36]	0.3460	0.3223	0.3013	0.2847	0.2597	0.2220	0.1726

Table 6. Normalized SIFs K_2 for rectangular plates containing central interface cracks at various inclination angles under uniform load.

	E_1:E_2	a/W						
		0.2	0.3	0.4	0.5	0.6	0.7	0.8
$\alpha = 45°$	10:1	0.4382	0.4364	0.4327	0.4302	0.4272	0.4224	0.4165
	5:1	0.3814	0.3795	0.3756	0.3682	0.3633	0.3617	0.3567
	2:1	0.2129	0.2121	0.2110	0.2105	0.2104	0.2096	0.2075
$\alpha = 30°$	10:1	0.4379	0.4338	0.4298	0.4269	0.4205	0.4195	0.4117
	5:1	0.3780	0.3751	0.3726	0.3698	0.3694	0.3681	0.3562
	2:1	0.2102	0.2097	0.2088	0.2082	0.2077	0.2066	0.2048
$\alpha = 15°$	10:1	0.4311	0.4282	0.4226	0.4222	0.4179	0.4144	0.4105
	5:1	0.3762	0.3717	0.3632	0.3586	0.3529	0.3516	0.3468
	2:1	0.2083	0.2078	0.2068	0.2063	0.2054	0.2035	0.2020
$\alpha = 0°$	10:1	0.4282	0.4252	0.4197	0.4188	0.4169	0.4108	0.4035
	5:1	0.3661	0.3642	0.3589	0.3587	0.3533	0.3516	0.3478
	2:1	0.2061	0.2056	0.2050	0.2035	0.2025	0.2016	0.2008

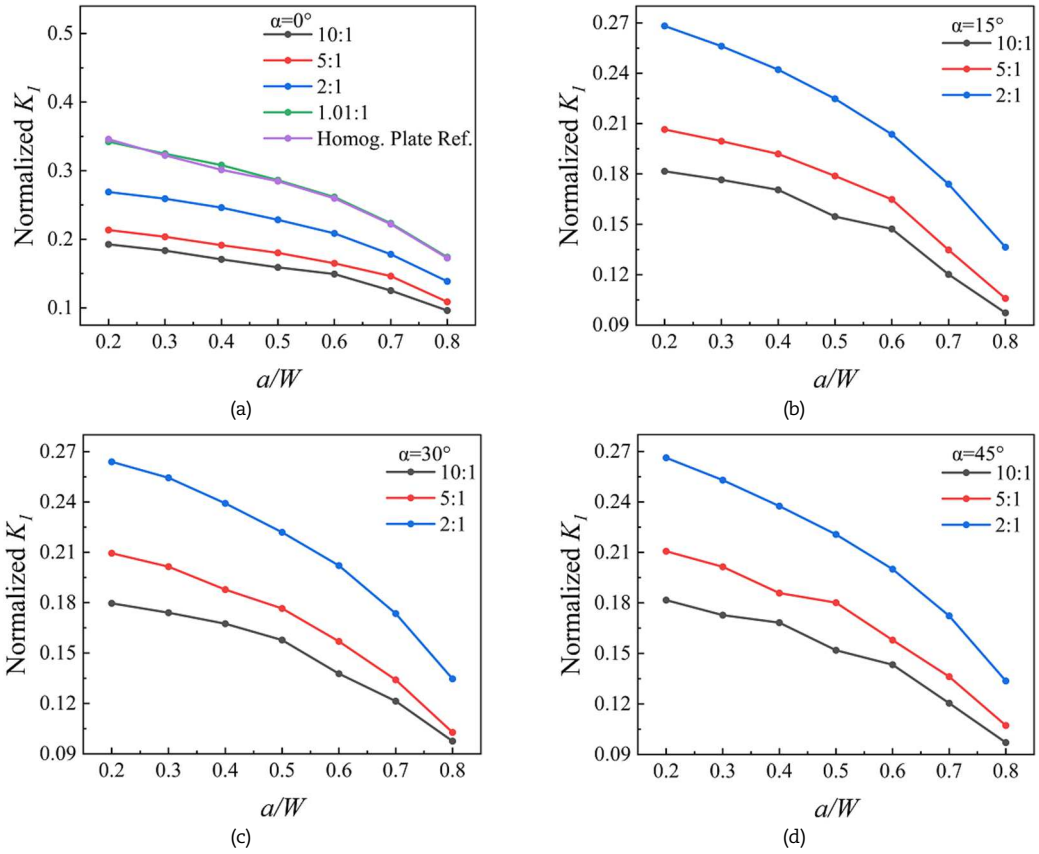


Fig. 9. Normalized SIFs K_1 for rectangular plates containing central interface cracks at various inclination angles under uniform load: (a) $\alpha = 0°$; (b) $\alpha = 15°$; (c) $\alpha = 30°$; (d) $\alpha = 45°$.

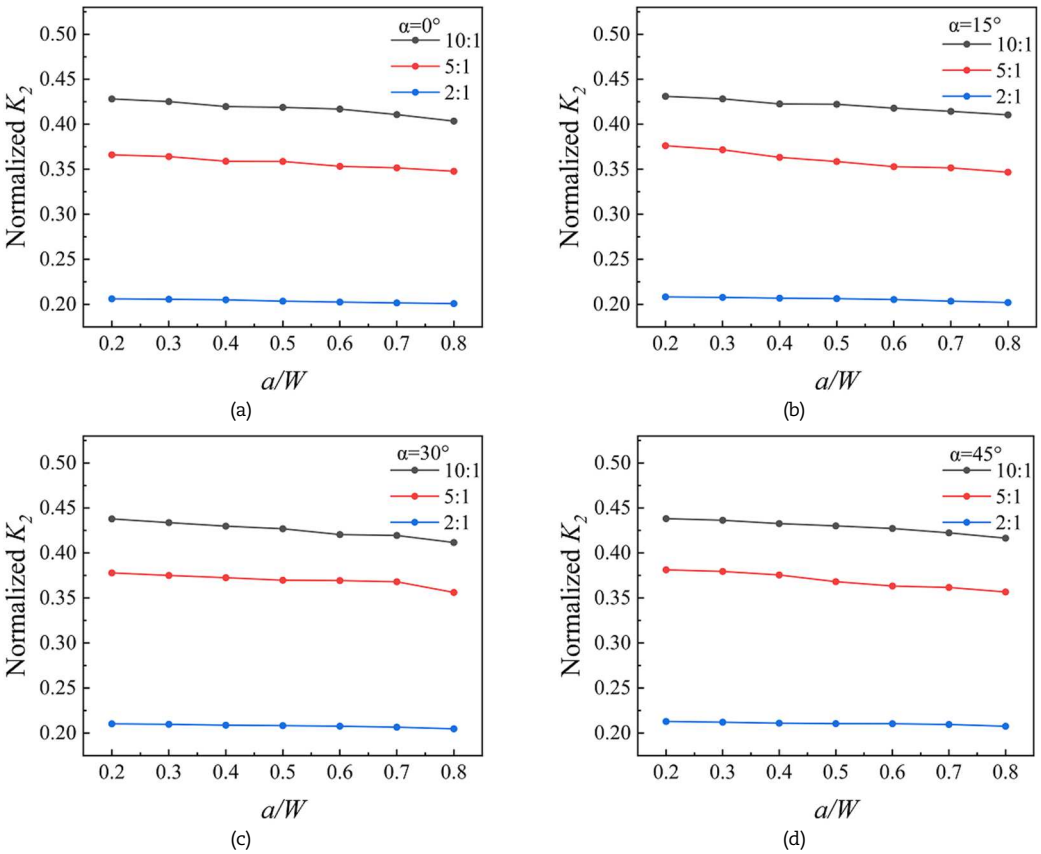


Fig. 10. Normalized SIFs K_2 for rectangular plates containing central interface cracks at various inclination angles under uniform load: (a) $\alpha = 0°$; (b) $\alpha = 15°$; (c) $\alpha = 30°$; (d) $\alpha = 45°$.

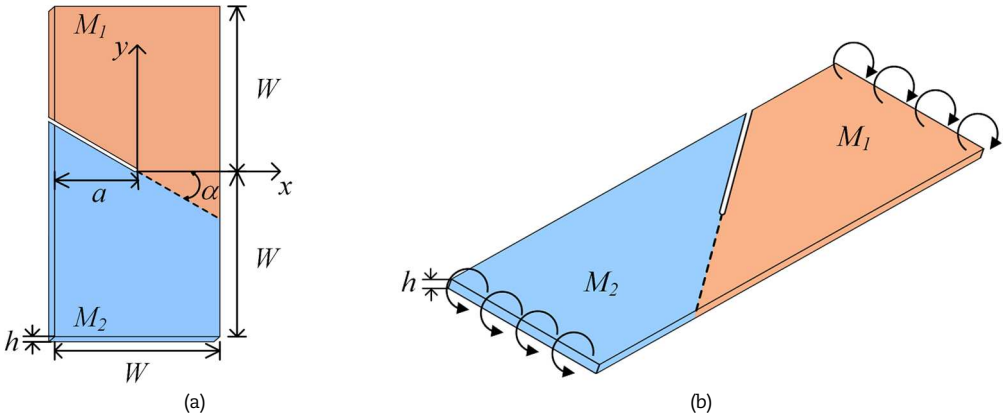


Fig. 11. (a) Rectangular plate with edge interface cracks; (b) Rectangular plate with edge interface cracks under bending moment.

5.3. Rectangular plate with an edge interface crack

Consider a rectangular plate of width W and height 2W, containing an inclined edge interface crack. As shown in Fig. 11(a), the crack is characterized by its projected length a and inclination angle α, where a denotes the perpendicular distance from the crack tip to the plate edge. The plate is subjected to a bending moment applied along its upper and lower boundaries, as illustrated in Fig. 11(b). The normalization factor for this case is $M\sqrt{\pi a}/h^2$. For Poisson's ratios of $\upsilon_1 = \upsilon_2 = 0.3$, the variation of normalized SIFs K_1 and K_2 with the elastic modulus ratio and crack length for different inclination angles are summarized in Tables 7 and 8. Both K_1 and K_2 increase with crack length. As the crack inclination angle increases, K_1 decreases while K_2 increases. Similarly, a higher elastic modulus ratio leads to a decrease in K_1 but an increase in K_2. The variation of the SIFs with the structural parameters is illustrated in Figs. 12-13.

6. Conclusion

Based on the symplectic analytical solution, this paper proposes an extended finite element method (XFEM) to analyze the bending problem of bi-material thin plates with interfacial cracks. Within the framework of the Kirchhoff plate theory, the symplectic analytical solution for the bending problem of plates with interfacial cracks is derived, from which 16 independent deflection modes are systematically extracted. These independent modes are subsequently introduced as enrichment functions into the finite element displacement approximation. To accurately represent discontinuities, a modified Heaviside function is introduced to model the crack surfaces, and level-set functions are employed to describe the material interface. Based on the principle of minimum potential energy, an extended finite element model for the bending problem of bi-material plates is established.

Table 7. Normalized SIFs K_1 for rectangular plates containing edge interface cracks at various inclination angles under bending moments.

	E_1:E_2	a/W						
		0.2	0.3	0.4	0.5	0.6	0.7	0.8
$\alpha = 45°$	10:1	2.0884	2.2523	2.4709	2.7426	3.0958	3.4784	3.9163
	5:1	2.2855	2.4338	2.6757	2.9698	3.3183	3.7346	4.2733
	2:1	2.8617	3.0165	3.2461	3.5628	3.9734	4.5128	5.1562
$\alpha = 30°$	10:1	2.6875	2.8085	3.0113	3.2938	3.6612	4.0825	4.5694
	5:1	2.9382	3.0506	3.2405	3.5446	3.9324	4.3819	4.9699
	2:1	3.7425	3.8799	4.1642	4.5241	5.0318	5.6419	6.4692
$\alpha = 15°$	10:1	3.0738	3.2156	3.3965	3.6379	3.9816	4.4128	4.9801
	5:1	3.3844	3.5099	3.7165	3.9883	4.3746	4.8095	5.4717
	2:1	4.3849	4.5515	4.8058	5.1823	5.6538	6.2722	7.0906
$\alpha = 0°$	10:1	3.1367	3.2246	3.3217	3.5051	3.7816	4.2467	4.7625
	5:1	3.5509	3.6375	3.7847	3.9795	4.3265	4.8192	5.4965
	2:1	4.5833	4.6832	4.8847	5.1383	5.5827	6.2759	7.1923

Table 8. Normalized SIFs K_2 for rectangular plates containing edge interface cracks at various inclination angles under bending moments.

	E_1:E_2	a/W						
		0.2	0.3	0.4	0.5	0.6	0.7	0.8
$\alpha = 45°$	10:1	4.3587	4.7134	5.3107	6.2150	7.2368	8.3799	9.4699
	5:1	4.0140	4.2388	4.6447	5.2817	6.0404	6.8432	7.7977
	2:1	3.6678	3.8099	4.0337	4.3264	4.6686	5.1201	5.6246
$\alpha = 30°$	10:1	3.6576	3.9337	4.3597	4.9218	5.5405	6.3092	7.0972
	5:1	3.4238	3.6229	3.9479	4.3298	4.8132	5.3173	5.8096
	2:1	3.1477	3.2821	3.4302	3.6154	3.8513	4.0912	4.4164
$\alpha = 15°$	10:1	2.1067	2.2303	2.4238	2.6956	3.0039	3.3466	3.7233
	5:1	1.9686	2.0568	2.1968	2.3994	2.6273	2.8730	3.1391
	2:1	1.8067	1.8692	1.9489	2.0451	2.1368	2.2667	2.4179
$\alpha = 0°$	10:1	1.0526	1.1404	1.2758	1.4137	1.6124	1.8181	2.0629
	5:1	0.7876	0.8483	0.9227	1.0237	1.1289	1.2795	1.4581
	2:1	0.4992	0.5377	0.5669	0.6235	0.6874	0.7812	0.8821

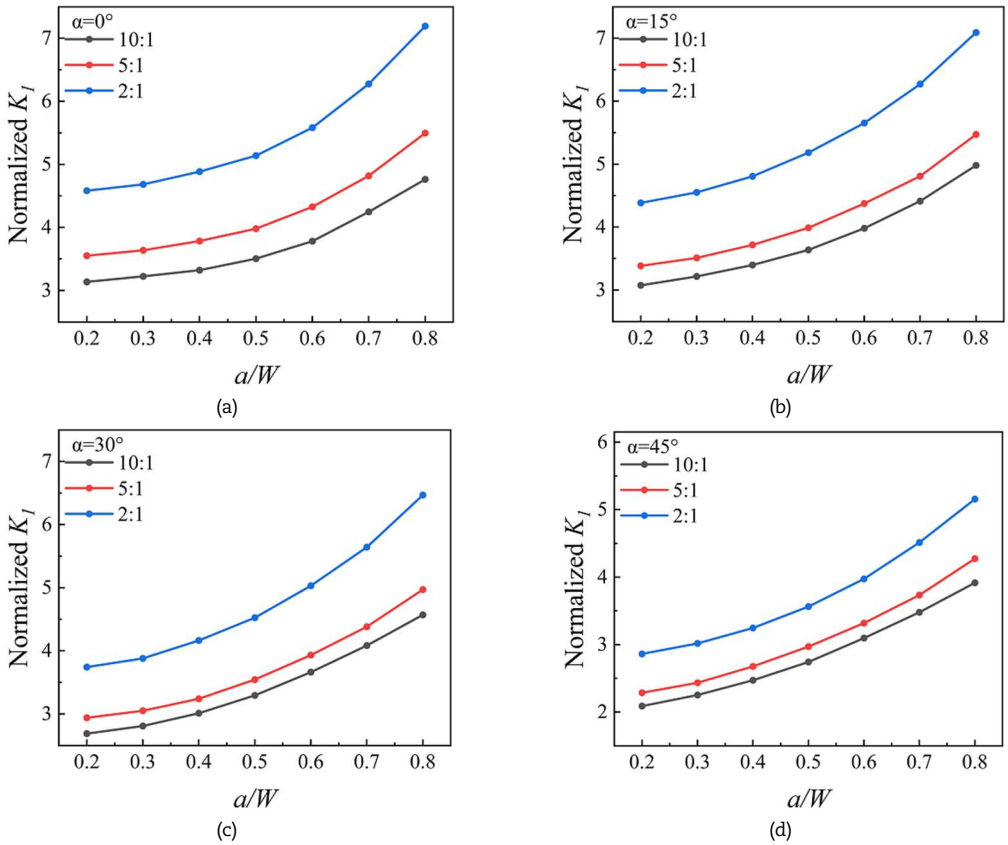


Fig. 12. Normalized SIFs K_1 for rectangular plates containing edge interface cracks at various inclination angles under bending moments: (a) $\alpha = 0°$; (b) $\alpha = 15°$; (c) $\alpha = 30°$; (d) $\alpha = 45°$.

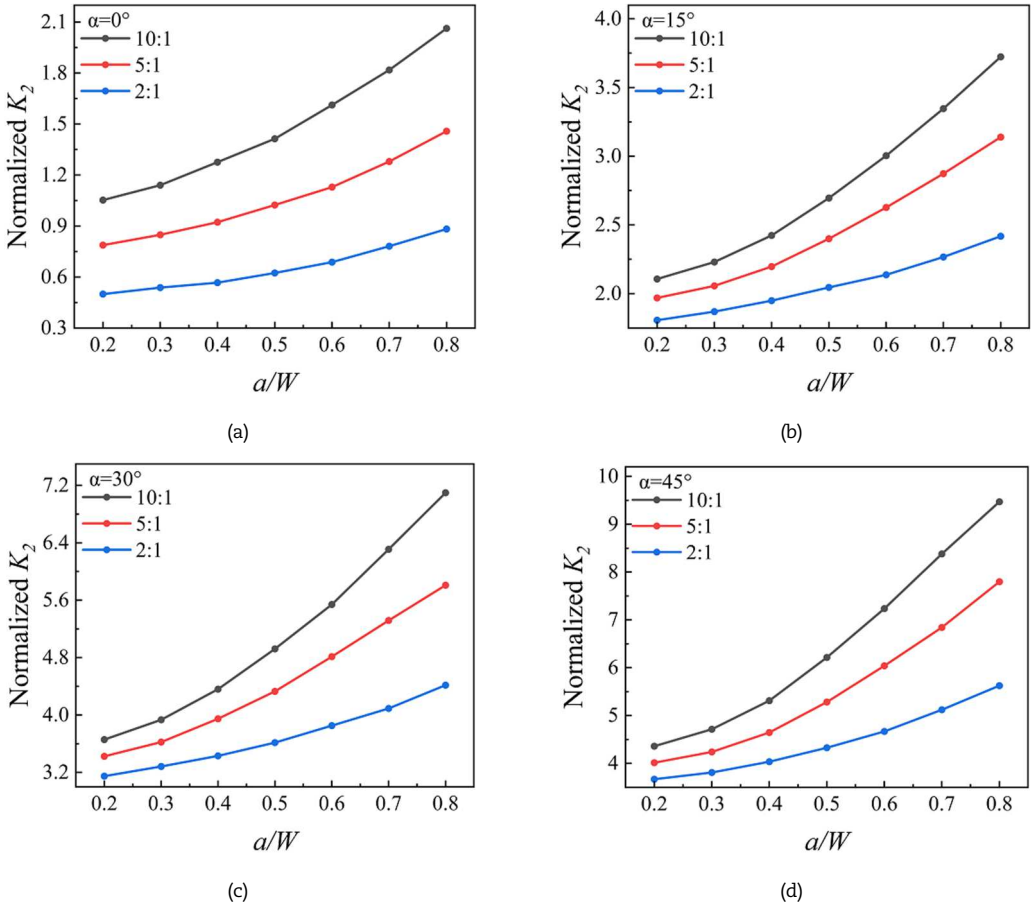


Fig. 13. Normalized SIFs K_2 for rectangular plates containing edge interface cracks at various inclination angles under bending moments: (a) $\alpha = 0°$; (b) $\alpha = 15°$; (c) $\alpha = 30°$; (d) $\alpha = 45°$.

The conventional element adopted is the discrete Kirchhoff theory (DKT) element, which is a three-node triangular element using area coordinates as parametric coordinates and is capable of discretizing plate structures with arbitrary geometries. The stress intensity factors (SIFs) at the interfacial crack tip are calculated using the interaction integral method. In this method, the physical field in the actual state is computed using the proposed XFEM, while the auxiliary field is obtained from the symplectic analytical solution. The SIFs are then extracted by evaluating the contour integral of the interaction energy. Comparisons with existing results in the literature demonstrate that the proposed method can yield accurate SIFs. In addition, new numerical results for several previously unstudied plate structures are provided.

The proposed symplectic analytical-XFEM model is applicable to the bending fracture analysis of Kirchhoff thin plates. Its advantage lies in introducing 16 symplectic series enrichment functions with oscillatory characteristics, which can capture the stress singularity at the bi-material interfacial crack tip with high precision; meanwhile, XFEM avoids mesh reconstruction and enables accurate determination of SIFs. However, the model is restricted by the classical thin plate assumption and neglects transverse shear deformation, making it difficult to directly apply to the analysis of moderately thick plates. Furthermore, its assumptions of an ideally bonded interface and linear elastic constitutive law limit its application to weakly bonded interfaces, multi-material systems, and elastoplastic fracture problems.

Author Contributions

W. Xu planned the scheme, initiated the project, and developed the mathematical modeling; J. Chen wrote the original draft, conducted the simulations and analyzed the results; Y. Xu contributed to investigation and suggested the methods; L. Li was responsible for writing review and editing; D. Zhong contributed to supervision and formal analysis. The manuscript was written through the contribution of all authors. All authors discussed the results, reviewed, and approved the final version of the manuscript.

Acknowledgments

Not applicable.

Conflict of Interest

The authors declared no potential conflicts of interest concerning the research, authorship, and publication of this article.

Funding

The authors received no financial support for the research, authorship, and publication of this article.

Data Availability Statements

No new datasets were generated during this study. All numerical results and simulation models supporting the findings are included in the article and supplementary materials.

Appendix A

For the bending problem of a bi-material plate with an interface crack, the coefficients $A^{(i)}, B^{(i)}, C^{(i)}, G^{(i)}$ in the symplectic analytical solution must satisfy the following relationships:

$$\left\{A^{(2)},B^{(2)},C^{(2)},G^{(2)}\right\}^{\mathrm{T}}=\beta\left\{A^{(1)},B^{(1)},C^{(1)},G^{(1)}\right\}^{\mathrm{T}} \tag{A1}$$

where,

$$\beta=\left[\beta_{ij}\right],\ \gamma=\left[\gamma_{ij}\right],\ \beta_{12}=\beta_{14}=\beta_{21}=\beta_{23}=\beta_{32}=\beta_{34}=\beta_{41}=\beta_{43}=0,$$

$$\beta_{11}=\frac{1-\upsilon_2}{4}\left[1+\mu+\frac{\lambda(3+\upsilon_2-\mu+\upsilon_2\mu)}{1-\upsilon_1}\right],$$

$$\beta_{13}=\frac{(1-\upsilon_2)(1+\mu)\left[3+\upsilon_1-\mu+\upsilon_1\mu-\lambda(3+\upsilon_2-\mu+\upsilon_2\mu)\right]}{4(3+\upsilon_1+\mu-\upsilon_1\mu)},$$

$$\beta_{22}=\frac{1-\upsilon_2}{4}\left[1-\mu+\frac{\lambda(3+\upsilon_2+\mu-\upsilon_2\mu)}{1-\upsilon_1}\right],$$

$$\beta_{24}=\frac{(1-\upsilon_2)(1-\mu)}{4}\left[1-\frac{\lambda(3+\upsilon_2+\mu-\upsilon_2\mu)}{3+\upsilon_1+\mu-\upsilon_1\mu}\right],$$

$$\beta_{31}=\beta_{42}=\frac{3+\upsilon_2+\mu-\upsilon_2\mu}{4}\left[1-\frac{\lambda(1-\upsilon_2)}{1-\upsilon_1}\right],$$

$$\beta_{33}=\frac{(3+\upsilon_2+\mu-\upsilon_2\mu)\left[3+\upsilon_1-\mu+\upsilon_1\mu+\lambda(1+\mu)(1-\upsilon_2)\right]}{4(3+\upsilon_1+\mu-\upsilon_1\mu)},$$

$$\beta_{44}=\frac{3+\upsilon_2+\mu-\upsilon_2\mu}{4}\left[1+\frac{\lambda(1-\upsilon_2)(1-\mu)}{3+\upsilon_1+\mu-\upsilon_1\mu}\right],\ \lambda=\frac{D^{(2)}}{D^{(1)}}.$$

Meanwhile, the coefficients of the symplectic analytical series in Material 1 must satisfy:

$$\gamma\left\{A^{(1)},B^{(1)},C^{(1)},G^{(1)}\right\}^{\mathrm{T}}=\mathbf{0} \tag{A2}$$

where,

$$\gamma_{11}=-\gamma_{22}=-\gamma_{24}=\gamma_{31}=-\gamma_{42}=-\gamma_{44}=\cos\mu\pi,$$

$$\gamma_{12}=\gamma_{21}=-\gamma_{23}=-\sin\mu\pi,\ \gamma_{13}=\gamma_{33}=\zeta_1\cos\pi,$$

$$\gamma_{14}=\zeta_1\sin\mu\pi,\ \gamma_{32}=\gamma_{41}=\zeta_2\sin\mu\pi,\ \gamma_{34}=\zeta_3\sin\mu\pi,$$

$$\gamma_{43}=\zeta_4\sin\mu\pi,\ \ \zeta_1=\frac{3+\upsilon_1-\mu+\upsilon_1\mu}{3+\upsilon_1+\mu-\upsilon_1\mu},\ \zeta_2=-\frac{1}{2}\left[1+\upsilon^{(2)}-\frac{\lambda\left(1-\upsilon^{(2)}\right)\left(3+\upsilon^{(2)}\right)}{1-\upsilon^{(1)}}\right],$$

$$\zeta_3=-\frac{1}{2}\left[1+\upsilon^{(2)}+\frac{\lambda(1-\mu)\left(1-\upsilon^{(2)}\right)\left(3+\upsilon^{(2)}\right)}{3+\upsilon^{(1)}+\mu-\upsilon^{(1)}\mu}\right],$$

$$\zeta_4=-\frac{1}{2}\left[\frac{\left(3+\upsilon^{(1)}-\mu+\upsilon^{(1)}\mu\right)\left(1+\upsilon^{(2)}\right)+\lambda(1+\mu)\left(1-\upsilon^{(2)}\right)\left(3+\upsilon^{(2)}\right)}{3+\upsilon^{(1)}+\mu-\upsilon^{(1)}\mu}\right].$$

Reference

[1] Irwin G.R., Analysis of stresses and strains near the end of a crack traversing a plate, *Journal of Applied Mechanics*, 24(3), 1957, 361-364.
[2] Williams M.L., The bending stress distribution at the base of a stationary crack, *Journal of Applied Mechanics*, 28(1), 1961, 78-82.
[3] Sih G.C., Paris P.C., Erdogan F., Crack-tip stress-intensity factors for plane extension and plate bending problems, *Journal of Applied Mechanics,* 29(2), 1962, 306-312.
[4] Wang N.M., Effects of plate thickness on the bending of an elastic plate containing a crack, *Journal of Mathematics and Physics*, 47(1-4), 1968, 371-390.
[5] Hartranft R., Sih G., Effect of plate thickness on the bending stress distribution around through cracks, *Journal of Mathematics and Physics*, 47(1-4), 1968, 276-291.
[6] Barsoum R.S., A degenerate solid element for linear fracture analysis of plate bending and general shells, *International Journal for Numerical Methods in Engineering*, 10(3), 1976, 551-564.
[7] Chen W.H., Yang K.C., Chang C.S., A finite element alternating approach for the bending analysis of thin cracked plates, *International Journal of Fracture*, 56(2), 1992, 93-110.
[8] Leung A.Y.T, Su R. , Fractal two-level finite element method for cracked Kirchhoff's plates using DKT elements, *Engineering Fracture Mechanics*, 54(5), 1996, 703-711.
[9] Park J.H., Atluri S.N., Analysis of a cracked thin isotropic plate subjected to bending moment by using FEAM, *KSME International Journal*, 13(12), 1999, 912-917.
[10] Moës N., Dolbow J., Belytschko T., A finite element method for crack growth without remeshing, *International Journal for Numerical Methods in Engineering*, 46(1), 1999, 131-150.
[11] Munaswamy K., Pullela R., Computation of stress intensity factors for through cracks in plates using p-version finite element method, *Communications in Numerical Methods in Engineering*, 24(12), 2008, 1753-1780.
[12] Leung A.Y.T, Zhou Z., Xu X., Determination of stress intensity factors by the finite element discretized symplectic method, *International Journal of Solids and Structures*, 51(5), 2014, 1115-1122.
[13] Nguyen N.T., Lo V.S., Nguyen D.K., Truong T.T., An improved extended integrated radial basis functions meshfree method for dynamic fracture analysis in bending plate structure, *Engineering Analysis with Boundary Elements*, 166, 2024, 105804.
[14] Suo Z., Hutchinson J.W., Interface crack between two elastic layers, *International Journal of Fracture*, 43(1), 1990, 1-18.
[15] Ambrico J.M., Jones E.E., Begley M.R., Cracking in thin multi-layers with finite-width and periodic architectures, *International Journal of Solids and Structures*, 39(6), 2002, 1443-1462.
[16] Sih G.C., Rice J.R., The bending of plates of dissimilar materials with cracks, *Journal of Applied Mechanics*, 31(3), 1964, 477-482.
[17] Perlman A., Sih G., Circular-arc cracks in bi-material plates under bending, *International Journal of Fracture Mechanics*, 3(3), 1967, 193-206.
[18] Chen W.H., Hwu C.B., Hybrid singular element design for the bending analysis of bimaterial thin cracked plates, *AIAA Journal*, 24(8), 1986, 1399-1402.
[19] Kakuno H., Oda K., Morisaki T., Analysis of stress intensity factor for interfacial crack in bonded dissimilar plate under bending, *Key Engineering Materials*, 417, 2010, 153-156.
[20] Oda K., Lan X., Noda N.A., Michinaka K., Effect of arbitrary bi-material combination and bending loading conditions on stress intensity factors of an edge interface crack, *International Journal of Structural Integrity*, 3(4), 2012, 457-475.
[21] Yao W., Wang S., An analytical singular element for interface cracks in bi-material Kirchhoff plate bending, *Engineering Fracture Mechanics*, 91, 2012, 103-116.
[22] Jiang S., Gu Y., Fan C.M., Qu W., Fracture mechanics analysis of bimaterial interface cracks using the generalized finite difference method, *Theoretical and Applied Fracture Mechanics*, 113, 2021, 102942.
[23] Batoz J.L., Tahar M.B., Evaluation of a new quadrilateral thin plate bending element, *International Journal for Numerical Methods in Engineering*, 18(11), 1982, 1655-1677.
[24] Tian L., Cheng Z., A triangular plate bending element based on discrete Kirchhoff theory with simple explicit expression, *Mathematics*, 9(11), 2021, 1181.
[25] Batoz J.L., Bathe K.J., Ho L.W., A study of three-node triangular plate bending elements, *International Journal for Numerical Methods in Engineering*, 15(12), 1980, 1771-1812.
[26] Zi G., Belytschko T., New crack-tip elements for XFEM and applications to cohesive cracks, *International Journal for Numerical Methods in Engineering*, 57(15), 2003, 2221-2240.
[27] Ventura G., Benvenuti E., Equivalent polynomials for quadrature in Heaviside function enriched elements, *International Journal for Numerical Methods in Engineering*, 102(3-4), 2015, 688-710.
[28] Khurshudyan A.Z., An identity for the Heaviside function and its application in representation of nonlinear Green's function, *Computational and Applied Mathematics*, 39(1), 2020, 32.
[29] Zhu Q.Z., On enrichment functions in the extended finite element method, *International Journal for Numerical Methods in Engineering*, 91(2), 2012, 186-217.
[30] Williams M.L., On the stress distribution at the base of a stationary crack, *Journal of Applied Mechanics*, 24(1), 1957, 109-114.



[31] Yao W., Zhong W., Lim C.W., *Symplectic elasticity*, World Scientific, 2009.
[32] Dirac P.A.M., Generalized Hamiltonian Dynamics, *Canadian Journal of Mathematics*, 2, 1950, 129-148.
[33] Moran B., Shih C., Crack tip and associated domain integrals from momentum and energy balance, *Engineering Fracture Mechanics*, 27(6), 1987, 615-642.
[34] Sukumar N., Prévost J.H., Modeling quasi-static crack growth with the extended finite element method Part I: Computer implementation, *International Journal of Solids and Structures*, 40(26), 2003, 7513-7537.
[35] Yau J.F., Wang S.S., Corten H.T., A mixed-mode crack analysis of isotropic solids using conservation laws of elasticity, *Journal of Applied Mechanics*, 47(2), 1980, 335-341.
[36] Wang Y., Tham L., Lee P., Tsui Y., A boundary collocation method for cracked plates, *Computers & Structures*, 81(28-29), 2003, 2621-2630.
[37] Jiang C., Cheung Y., A special bending crack tip finite element, *International Journal of Fracture*, 71(1), 1995, 57-69.

ORCID iD

Wang Xu https://orcid.org/0009-0007-2708-088X

© 2026 Shahid Chamran University of Ahvaz, Ahvaz, Iran. This article is an open access article distributed under the terms and conditions of the Creative Commons Attribution-NonCommercial 4.0 International (CC BY-NC 4.0 license) (http://creativecommons.org/licenses/by-nc/4.0/).

How to cite this article: Xu W., et al. A Symplectic-Analysis-Based Extended Finite Element Method for Bending of Bi-Material Plates with Interface Cracks, *J. Appl. Comput. Mech.*, xx(x), 2026, 1–18. https://doi.org/10.22055/jacm.2026.49382.5936

Publisher's Note Shahid Chamran University of Ahvaz remains neutral with regard to jurisdictional claims in published maps and institutional affiliations.